Anatomical imaging for radiotherapy

2008 Phys. Med. Biol. 53 R151

(http://iopscience.iop.org/0031-9155/53/12/R01)

IOP PUBLISHING PHYSICS IN MEDICINE AND BIOLOGY

Phys. Med. Biol. **53** (2008) R151–R191 doi:10.1088/0031-9155/53/12/R01

TOPICAL REVIEW

Anatomical imaging for radiotherapy

Philip M Evans[1]

Joint Physics Department, Institute of Cancer Research and Royal Marsden NHS Foundation Trust, Downs Road, Sutton, Surrey SM2 5PT, UK

E-mail: phil.evans@icr.ac.uk

Received , in final form 16 April 2008
Published 21 May 2008
Online at stacks.iop.org/PMB/53/R151

Abstract

The goal of radiation therapy is to achieve maximal therapeutic benefit expressed in terms of a high probability of local control of disease with minimal side effects. Physically this often equates to the delivery of a high dose of radiation to the tumour or target region whilst maintaining an acceptably low dose to other tissues, particularly those adjacent to the target. Techniques such as intensity modulated radiotherapy (IMRT), stereotactic radiosurgery and computer planned brachytherapy provide the means to calculate the radiation dose delivery to achieve the desired dose distribution. Imaging is an essential tool in all state of the art planning and delivery techniques: (i) to enable planning of the desired treatment, (ii) to verify the treatment is delivered as planned and (iii) to follow-up treatment outcome to monitor that the treatment has had the desired effect. Clinical imaging techniques can be loosely classified into anatomic methods which measure the basic physical characteristics of tissue such as their density and biological imaging techniques which measure functional characteristics such as metabolism. In this review we consider anatomical imaging techniques. Biological imaging is considered in another article. Anatomical imaging is generally used for goals (i) and (ii) above. Computed tomography (CT) has been the mainstay of anatomical treatment planning for many years, enabling some delineation of soft tissue as well as radiation attenuation estimation for dose prediction. Magnetic resonance imaging is fast becoming widespread alongside CT, enabling superior soft-tissue visualization. Traditionally scanning for treatment planning has relied on the use of a single snapshot scan. Recent years have seen the development of techniques such as 4D CT and adaptive radiotherapy (ART). In 4D CT raw data are encoded with phase information and reconstructed to yield a set of scans detailing motion through the breathing, or cardiac, cycle. In ART a set of scans is taken on different days. Both allow planning to account for variability intrinsic to the patient. Treatment verification has been carried out using a variety of technologies including: MV portal imaging, kV

[1] Author for correspondence: Joint Physics Department, Royal Marsden Hospital, Downs Road, Sutton, Surrey, SM2 5PT, UK

portal/fluoroscopy, MVCT, conebeam kVCT, ultrasound and optical surface imaging. The various methods have their pros and cons. The four x-ray methods involve an extra radiation dose to normal tissue. The portal methods may not generally be used to visualize soft tissue, consequently they are often used in conjunction with implanted fiducial markers. The two CT-based methods allow measurement of inter-fraction variation only. Ultrasound allows soft-tissue measurement with zero dose but requires skilled interpretation, and there is evidence of systematic differences between ultrasound and other data sources, perhaps due to the effects of the probe pressure. Optical imaging also involves zero dose but requires good correlation between the target and the external measurement and thus is often used in conjunction with an x-ray method. The use of anatomical imaging in radiotherapy allows treatment uncertainties to be determined. These include errors between the mean position at treatment and that at planning (the systematic error) and the day-to-day variation in treatment set-up (the random error). Positional variations may also be categorized in terms of inter- and intra-fraction errors. Various empirical treatment margin formulae and intervention approaches exist to determine the optimum strategies for treatment in the presence of these known errors. Other methods exist to try to minimize error margins drastically including the currently available breath-hold techniques and the tracking methods which are largely in development. This paper will review anatomical imaging techniques in radiotherapy and how they are used to boost the therapeutic benefit of the treatment.

It is a very sad thing that nowadays there is so little useless information: Oscar Wilde

(Some figures in this article are in colour only in the electronic version)

Contents

1. Introduction

Modern radiotherapy uses high technology to try to achieve optimal local tumour control whilst minimizing treatment side effects to an acceptably low level. Aspects of the technology used for this goal include: computer systems for three-dimensional treatment planning and simulation, with accurate radiation dose deposition models and facilities for optimization of external radiation beam or brachytherapy source distribution; computer-controlled linear accelerators with dynamic beam collimation systems for external beam treatment or systems such as remote afterloading for brachytherapy; and the use of radiation response models to characterize the treatment outcome and to enable the prediction of treatment outcomes for future patients' treatments.

One of the cornerstones of the whole radiotherapy process is the use of information obtained from images. Imaging is needed at every stage of the whole treatment process to measure various aspects of the region of the patient being treated. The information obtained from the imaging may be used to diagnose the disease and to stage it, it may be used to provide input data for the treatment planning process, it may be used at the time of treatment to monitor the accuracy of the treatment (i.e. to ensure that the delivery of the radiation dose is anatomically correct) and it may be used to monitor response to treatment. Repeat images may be used at treatment planning and during the treatment to adapt to variations in patient behaviour, both random variations and those in response to treatment, in a process known as adaptive radiotherapy (ART). Thus imaging information obtained about the patient is vital to essentially every stage of the radiotherapy process. Figure 1 shows a schematic illustration of the use of imaging in radiotherapy. The two bold boxes are the focus of this review.

Imaging methods in radiotherapy may generally be grouped into two types. The first group is made up of those methods that provide anatomical information that is the amount of tissue in the beam but not the status of that tissue, i.e. whether it is viable or not. Examples include conventional computed tomography (CT) and magnetic resonance imaging (MRI). CT produces a map of x-ray attenuation coefficients at the energy used to perform the scan, which with appropriate scaling or conversion factors gives a good approximation to density. MRI most commonly gives a proton density map of the tissue. The second group are those imaging methods that measure some functional or biological aspect of the tissue being imaged. Examples include radionuclide imaging such as single photon emission tomography (SPECT) or positron emission tomography (PET) and magnetic resonance spectroscopy (MRS). This review discusses only the application of anatomical imaging in radiotherapy. Biological, or functional, imaging is considered in a separate review by Nestle *et al* (2008). Dynamic contrast imaging with CT, MRI and other modalities might be argued to be anatomical and functional. For simplicity these applications are considered in this review rather than that of Nestle *et al*.

Whilst imaging information is used to determine the location of tissue to be treated to high radiation dose and, to a great extent, the value of that dose, the imaging process has limitations that need to be considered. Firstly, when imaging to define the tumour position and extent, the skill of the observer is important in delineating tumour from adjacent normal tissue. This is a task which can be extremely difficult as shown by variations between imaging techniques and between observers using the same technique. Also a given image only represents a snapshot of the patient's anatomy and the position of that anatomy. Thus consideration is needed that the imaging information has uncertainty associated with it, in regard to how typically a picture it paints of the position of tissues during treatment, with respect to variations between planning scans and treatment, day-to-day variations during treatment and movement effects during a single treatment visit. Other uncertainties exist with regard to how clearly the edges of target and non-target tissues may be determined in the image. Often these sources of uncertainties

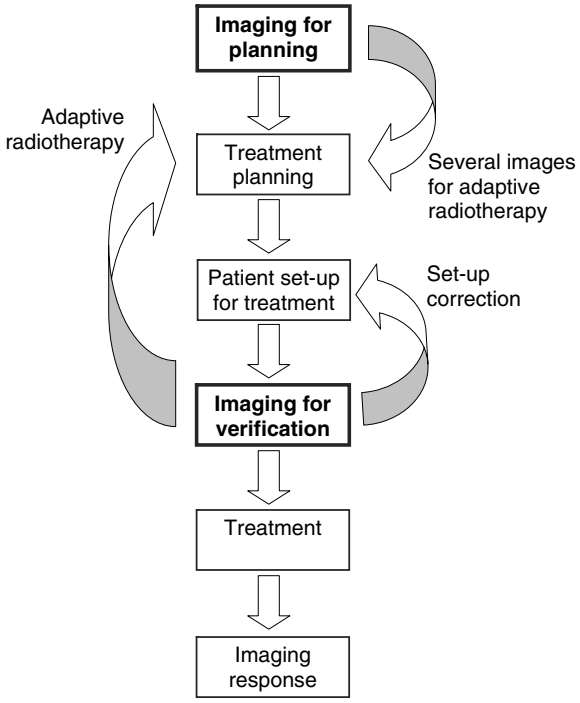

Figure 1. Illustration of the use of imaging in the radiotherapy treatment chain. The boxes in bold are the focus of this review. The use of multiple images and imaging feedback in the treatment planning process and for set-up correction are illustrated by curved arrows.

are accounted for by using geometric margins, the nature of which depends on the type of uncertainty to be accounted for (McKenzie *et al* 2000, 2002, van Herk 2004).

The use of imaging for cancer diagnosis and staging is a huge area worthy of review in itself, and in the limited space of this review the focus will be on the use of anatomical imaging once the diagnosis and staging process has been completed. Firstly, the relationship between imaging, organ localization, errors and treatment margins will be discussed. The next process to be considered is that of treatment planning with anatomical imaging, in which, most commonly, CT and MR data are used to localize the tumour, then margins for error are defined around the localized tumour to produce a target and finally external radiation beams, or brachytherapy source positions, are designed to produce the desired dose distribution. Then how anatomical imaging contributes to the process of treatment verification, in which the anatomical positioning accuracy and dosimetric accuracy of the treatment must be measured (and ideally corrected) for each treatment fraction, is reviewed. The measurement of treatment outcome using imaging is a large area, in which biological imaging is playing a greater part. This is beyond the scope of this review.

2. Imaging and treatment uncertainties

The purpose of anatomical imaging in radiotherapy is to determine the position of the target, either to localize and delineate it in the planning stage or to verify it during treatment. The snapshot provided by a single image may not be accurate for all stages during the treatment course. Of the various errors present in radiotherapy, several of them are attributable to the

limitations of the process of planning a treatment based on imaging information which involves skilled interpretation and which is obtained before treatment.

(1) The anatomical image contains no functional information; hence if the density of tumour and normal tissue is similar in the image, definition of the tumour may be difficult.
(2) The anatomy in the planning image may not be completely indicative of the anatomy during treatment. This may be the result of a change in patient weight or a positional different between the planning scan and the mean treatment position. Both of these lead to a systematic error in the treatment (Hurkmans *et al* 2001, van Herk 2004).
(3) There are stochastic variations in position from day-to-day in fractionated external beam treatment. Anatomical imaging may be used to measure and/or correct for these inter-fraction treatment errors (Hurkmans *et al* 2001, van Herk 2004).
(4) Particularly in the case of treatment in the thorax, intra-fraction variations may occur as a result of processes such as the breathing and cardiac cycles. Imaging may be used to characterize the resultant pattern of motion, so that treatment strategies can be designed to account for it (Seppenwoolde *et al* 2002, 2007, Shirato *et al* 2004b, 2006).
(5) Time trends may occur in fractioned treatments. This may be due to weight change or the response of tissue to radiation (Elgayed *et al* 1993, Hector *et al* 2000, McDermott *et al* 2006). The treatment should ideally respond to such changes.

The various errors have different effects on the treatment and thus may have to be dealt with differently.

On the whole, the distributions of systematic and random inter-fraction variations are thought to be stochastic and follow a Gaussian distribution (McKenzie *et al* 2000, van Herk 2004). Simulation techniques have been used to calculate margins needed to achieve a desired treatment accuracy (minimum percentage of tissue volume receiving a minimum dose level when summed over all treatment fractions) as a function of the systematic and random error distribution (Stroom *et al* 1999, van Herk *et al* 2000). These show the systematic error to be approximately three times as important as the random component. Correction strategies have been developed to reduce set-up margins. These fall into two categories: online protocols, in which both systematic and random errors are reduced by imaging with a test dose at the start of each treatment fraction and correcting set-up based on anatomical position (De Neve *et al* 1992, Ezz *et al* 1992, Gildersleve *et al* 1994), and offline, in which a set of images are acquired to determine the systematic error component, which is then corrected at the next fraction. Various offline protocols have been developed, including the shrinking action level (SAL) and the no action level (NAL) (Bel *et al* 1993, De Boer and Heijmen 2001, 2007).

The data for breathing motion are generally not normally distributed. Often the temporal distribution has a minimum in the centre, with maxima at exhale and inhale and shows variability from cycle to cycle (Ford *et al* 2002a). Thus it is distinctly non-Gaussian. However, the fact that the treatment is fractionated ameliorates the problem in that a consequence of the central limit theorem is that the average over a sufficient number of fractions (typically 30) is Gaussian (Bortfeld *et al* 2002). This requires that the breathing phase is asynchronous with the treatment delivery system. Nevertheless, treatment errors may still ensue due to the fact that a single (or a few) snapshot of the breathing distribution is sampled when anatomical images are obtained for planning. This may introduce systematic treatment errors unless sufficient imaging data are acquired to describe the breathing distribution (Evans *et al* 2006a). Another potential source of error is in the case of IMRT delivery with small segment doses, which can lead to beating between the patient motion and beam segment delivery (Seco *et al* 2007). The complexity of intra-fraction motion has lead to a variety of approaches to its management, including using large margins to encompass its extent, breath hold, both

voluntary and controlled (Lu *et al* 2000, Wong *et al* 1999, Remouchamps *et al* 2003, Hanley *et al* 1999, Mageras and Yorke 2004), treatment delivery gating (Kubo and Hill 1996, Shirato *et al* 2000b, Minohara *et al* 2000) and delivery tracking (McQuaid and Webb 2006).

This discussion has focused on the relationship between the accuracy and quantity of the information from anatomic imaging and the margins for error needed. It should be emphasized that whilst good anatomical imaging for treatment planning and verification helps control many of these errors, there are many sources of error (and hence components of the treatment margins) that are not identifiable solely with anatomic imaging. Examples include the use of biological imaging to define the gross tumour volume (GTV) (ICRU 50 and 62, Grosu *et al* 2005). Biological imaging may also improve definition of the margin to determine the clinical target volume (CTV). In the nomenclature of ICRU report 62, the set-up margin (SM) may include non-anatomical components, such as small differences in the coordinate frame used in the treatment machine and the treatment planning system (Van Herk 2004).

That aside, anatomical imaging has been used to achieve GTV definition and to monitor the treatment in various stages to allow small SM and internal margin (IM) parameters. A major challenge is to obtain sufficient information to characterize the behaviour of tumour and nearby normal tissues in the presence of the types of variations listed at the start of this section.

3. Anatomical imaging in treatment planning

Tumour definition is the first stage in the treatment planning process. Traditionally, this has been carried out for some treatment sites using planar x-ray imaging. With the advent of volumetric imaging (Hounsfield 1973, Mansfield 2004) and the development of methods of achieving complex dose distributions (Brahme 1988, Webb 1989, 2000), three-dimensional planning using volumetric information is now commonplace. In the chain of processes in a radiotherapy treatment, tumour definition is the most critical. It is often the link in the chain with the biggest uncertainty and, by the very nature of tumour definition, is a process usually carried out once, and consequently any errors at this stage propagate systematically throughout the whole treatment (Van Herk 2004).

Often the outline of the tumour is delineated manually on the imaging data, relying on skilled interpretation to distinguish tumour from non-tumour tissue with often low contrast and unclear boundaries. Studies have evaluated the accuracy of this process by comparing outlines produced by sets of observers to measure inter-observer variability and repeated outlines by a single observer to measure intra-observer variability, with results showing large variation in some cases. Methods of improving the variability in outlining have included combining different types of images, such as CT and MRI, and functional imaging such as PET. The combination of imaging methods in multimodality imaging requires registration of the various imaging datasets in the frame of reference of the treatment. Many approaches exist in the literature, from rigid body registration to deformable morphing of datasets. In addition fiducial markers, either external to the patient, or implanted close to the tumour, have been used either to aid image registration or to improve the accuracy of delineation in a single modality. Multimodality imaging is generally used to improve delineation of a static target by combining information.

Other approaches exist to ameliorate the target definition problem. These include the use of fixation systems and implanted markers. Fixation systems include external systems such as treatment-site-dependent boards (Creutzberg *et al* 1993), evacuated bean bags (Nalder *et al* 2001) and frames (Gill *et al* 1991) and internal systems such as catheters (Fransson *et al* 2002) and obturators (Merrick *et al* 1999). Implanted markers may be fiducial gold grains which

may be implanted using a biopsy needle (in the case of sites such as the prostate) (Crook *et al* 1995). Surgical clips may also be used at the time of surgery (in the case of the breast) (Machtay *et al* 1994, Marks *et al* 1994).

The effects of anatomical variations, both day-to-day and intra-fraction, may be measured by the acquisition of multiple datasets from the same modality. Day-to-day variations may be measured using repeat scans in a process known as adaptive radiotherapy or ART (Yan *et al* 1998). Intra-fraction variations, such as breathing effects, may be measured in CT by scanning sufficiently slowly to encompass the whole breathing cycle, but this introduces distortion to the image dataset. Alternatively, it may be measured using 4D imaging, in which data are acquired throughout the breathing cycle, with a measurement of the breathing phase so that the data may be sorted into different breathing phases to measure these variations.

The three main anatomical imaging methods used for target delineation in treatment planning are CT, MRI and ultrasound. We now consider each of these methods in turn, focussing on each of their use for target volume delineation and other considerations specific to their use in radiotherapy planning, including dose calculation.

3.1. Computed tomography

X-ray computed tomography (CT) has been a key component of radiotherapy diagnosis and planning from the time it was introduced into clinical practice in the early 1970s. A thorough review of x-ray computed tomography may be found in Kalender (2006). CT was the first imaging modality to offer detailed imaging of internal anatomy in three dimensions and thus to allow accurate determination of the spatial location of target tissues relative to non-target tissues.

Its role has evolved with the use of CT scans to calculate the attenuation of the treatment radiation (from an external beam or internal source) and the resultant dose distribution in the treatment planning process, along with the generation of reference image data for treatment verification in external beam treatment. These reference images, known as digitally reconstructed radiographs (DRRs), are projection x-ray images generated from the treatment-planning computer (Sherouse *et al* 1990) and may be compared with film or electronic portal images (EPI) for each treatment fraction.

We now consider the various aspects of the use of CT in treatment planning. Firstly, we consider aspects of target volume delineation, including the basic inter- and intra-observer variability of outlining the scans, the problems of outlining moving tumours, the use of CT perfusion to aid tumour visualization, the problems of artefacts in the scans due to metal implants and the problems of CT number calibration for planning and the use of multiple scans to achieve adaptive planning.

3.1.1. Target delineation. The primary purpose of CT scanning in radiotherapy is to enable delineation of the treatment target. This is often a difficult manual task and probably still the main source of inaccuracy in radiotherapy (Webb 1993). It is often difficult to obtain a ground truth measurement of tumour location, and manual outlining is the most common method of delineation. Thus the accuracy of the delineation process is usually described in several ways: intra-observer outlining variations, inter-observer variations and differences between imaging methods (such as between CT and MR and between CT and biological imaging (Nestle *et al* 2008)). The results are treatment site dependent. Here we summarize a few findings from the literature. A more detailed review of volumetric uncertainty in radiotherapy may be found in Hamilton and Ebert (2005).

One of the earliest studies of outlining variation was for the prostate and seminal vesicles (Fiorino *et al* 1998). Five well-trained radiotherapists contoured CT images of six patients scanned in the supine position. Outlining of one patient was repeated immediately to measure short-term intra-observer variability. The outlined volumes (referred to as inserted volumes) were estimated from lateral and antero-posterior projections in the beam's eye view. Intra-observer variability was relatively small, with an average variation of 5% (1 standard deviation (SD)). Inter-observer variation was larger 10–80% (1 SD). Variations were largest for the lateral margins of the prostate and seminal vesicles and the top and bottom of the prostate.

Inter-observer variability in lung tumour delineation has been studied by Van de Steene *et al* (2002). Five clinicians outlined the gross tumour volume (GTV) on CT scans of eight patients. The GTVs were compared in terms of the volume drawn and judgement of lymph node invasion. Clinical relevance of variations was evaluated using dose calculations in conformal treatment plans. The results showed inter-observer variations in tumour extent of between 2.8 and 7.3 cm. After common review of the lymph node status, it was found that there were 37% false negative and 22% false positive diagnoses, affecting the target volumes outlined.

Chang *et al* (2002) evaluated intra- and inter-observer variability for nasopharyngeal carcinoma. Thirteen patients were outlined by two trained observers. They found small differences between observers except in two cases with the involvement of the paranasal sinuses. Weiss *et al* (2003) evaluated target delineation by five radiation oncologists and two gynaecologists for three patients with cervical carcinoma. The ratio between largest and smallest volumes ranged between 3.6–4.9 and 1.3–2.8 for the radiation oncologists and for the gynaecologists respectively. The ratio of common volume to maximal encompassed volume (essentially the Jaccard similarity index (Tan *et al* 2005)) was respectively 0.11–0.13 and 0.30–0.57. Mukherji *et al* (2005) evaluated inter-observer variability for eight experienced observers outlining the GTV in squamous cell carcinoma of the supraglottic larynx. They found good agreement between the observers with a correlation coefficient of 0.81.

3.1.2. Image acquisition methods in the presence of motion. As discussed above the acquisition of a scan for treatment planning purposes represents a single snapshot of patient anatomy. Developments of the technology since the first demonstration of CT have included faster data acquisition and reconstruction time, with scanner rotation times now under half a second (Kalender 2006) and real-time reconstruction becoming possible with fast computers. In addition the advent of multi-slice scanners has enabled the imaging of large anatomical volumes in the time of a single rotation. Often the scanner operates in helical mode (Kalender *et al* 1989) for multi-slice acquisition. A major advantage of helical scanning over sequential slice acquisition is that moving objects (such as the heart or the breathing lungs) may be imaged continuously with a corresponding control of the resultant motion artefacts. At the time of writing 64 and 128 slice scanners represent the state of the art. Ultimately it is expected that a whole region of the body may be imaged with a single rotation (Lewis 2001). An alternative approach to the use of multiple fan slices is conebeam CT, using a two-dimensional detector (Feldkamp *et al* 1984) rather than a stack of one-dimensional detectors. This approach is particularly finding application for treatment verification (Jaffray *et al* 1999) as discussed later in this review. Advantages of the conebeam approach include potentially shorter acquisition times to image a volume. Disadvantages include greater difficulty in generating a scan calibrated in Hounsfield numbers due to the greater scatter component compared to the more conventional multiple slice detectors (Siewerdsen and Jaffray 2001). These improvements in scanner technology allow data acquisition with one or a few breath holds for imaging in the presence of lung motion (Kubo and Hill 1996).

Whilst imaging with breath hold greatly reduces motion artefacts in imaging mediastinum and lung tumours and is expected to aid diagnosis, it does not represent an ideal solution for treatment planning. External beam radiotherapy treatments generally take several minutes, during which a single breath hold is not possible. Several breath holds could be used but questions exist about the reproducibility of multiple breath holds (Wong *et al* 1999, Cheung *et al* 2003). Also there is the need for synchronization to treatment delivery (Kubo and Hill 1996). Technological developments are expected to ameliorate this problem, however, as treatment linac dose rates increase, partly due to the development of beams without flattening filters (Mackie *et al* 1999). In the case of brachytherapy a similar situation exists in that the treatment takes place over many breathing cycles.

An approach to generate CT data that are more representative of the distribution of tissue during the treatment is the use of a slow CT scan (Lagerwaard *et al* 2001, Wurstbauer *et al* 2005), the purpose of which is to sum over the motion in the breathing cycle and create an image showing the full tumour extent. Lagerwaard *et al* evaluated slow CT in comparison with conventional fast spiral scanning. Three conventional scans were also acquired during quiet expiration for 10 patients with peripheral lung tumours. Slice thickness was 3 mm, with the reconstruction index 2.5 mm. Three slow CT scans were acquired at 4 s/slice (slice thickness 4 mm, reconstruction index 3 mm). The images were registered and several measurements were made of the similarity of the volumes. In all cases the slow scan volume was larger than the conventional volume with an average increase of 14%. Slow CT was also found to be more reproducible. For each scan type, the ratio of the common overlapping volume to the volume encompassed by all three CTVs was evaluated (the Jaccard index). Values for this index of 54.9% $\pm$ 12.9% and 62.6% $\pm$ 10.8% were found for conventional fast and slow CT respectively, indicating the slow scans to be more reproducible.

Whilst slow CT used in this manner may improve over conventional, fast CT, it has the potential disadvantage in that it smears out the effects of movement, providing a motion envelope but not a temporal description of that motion. Four-dimensional computed tomography (4D CT) aims to measure the detailed motion of the tumour and thus to generate the probability density function of that motion, which may be used to improve treatment accuracy in several ways:

(1) to determine the centre of mass of the motion distribution and allow the minimization of the margin needed to account for that motion (Wolthaus *et al* 2006, Bortfeld *et al* 2002, Evans *et al* 2006a);

(2) to allow gating of the treatment in a particular phase of the breathing cycle (Balter *et al* 1998, Minohara *et al* 2000, Vedam *et al* 2001, Ford *et al* 2002a, Ozhasoglu *et al* 2002);

(3) to allow tracking of treatment delivery (Webb 2005, McQuaid and Webb 2006, McClelland *et al* 2007).

4D CT is used to acquire a detailed motion model of the patient's anatomy and particularly of the tumour for lung, oesophagus, liver and breast treatment. The currently available alternative techniques are subject to artefacts in the presence of breathing which 4D CT helps to avoid (Rietzel *et al* 2005a, 2005b, Jiang 2006). Consider a conventional scan of a breathing object, in which the scanner moves from top to bottom of the object when acquiring data. If the motion speed and scan speed are similar, then beating effects may occur. This has been illustrated by Rietzel for scanning of a moving sphere (figure 2, Rietzel *et al* 2005b). Depending on the synchronization between the scanner and the object, the sphere may appear distorted or as a set of disjointed objects. In the case of slow CT discussed above, the object distribution is convolved with the motion distribution to yield a blurred estimate. The use of

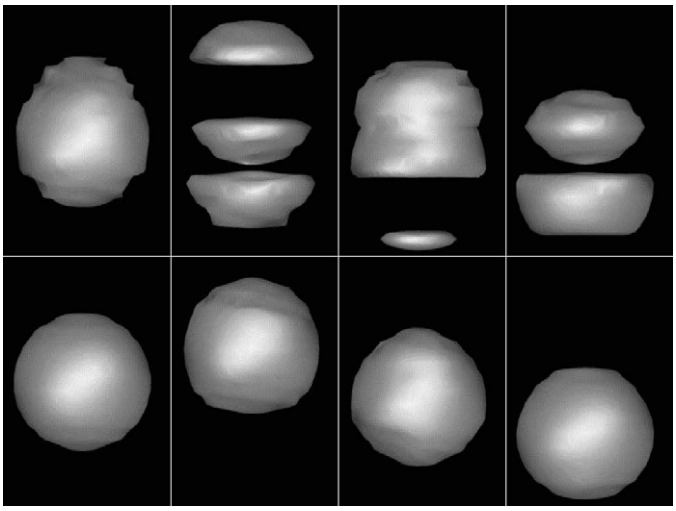

Figure 2. Isosurface rendering of a spherical object, CT scanned while periodically moving on a sliding table. Top row: different artefacts obtained by standard axial CT scanning starting at different motion phases. Bottom row: left shows a CT scan of the static object. Other images show three positions of the sphere while moving as imaged with 4D CT. Reproduced with kind permission from Rietzel *et al* (2005b).

such images for radiotherapy treatment planning results in a distorted target volume and hence a distorted dose distribution.

The requirement of 4D CT is to acquire raw data, often in a spiral scan geometry (or using the slow scan method), and to measure the position in the breathing cycle as the data are acquired (Ford *et al* 2002a, Low *et al* 2003, Keall 2004, Underberg *et al* 2004, Van der Geld *et al* 2006, Lu *et al* 2006b). This approach often involves using the cardiac gating input signal to the CT scanner (see for instance Ohnesorge *et al* (2000)). The data are binned into subsets based on breathing position and reconstructed separately to yield a set of snapshot images. Several methods of measuring position in the breathing cycle have been developed. Measurement of external anatomy has been used, including fluoroscopic video imaging of a marker placed on the skin, reported by Wagman *et al* (2003) and Keall *et al* (2004). One of the first examples of this includes the real-time position management (RPM) system which utilizes a marker incorporated into a block placed on the patient surface outside the treatment field, which is illuminated with infrared and the reflected light detected with a camera (Ford *et al* 2002a, Wagman *et al* 2003). Zhao *et al* (2007) have reported the use of an optical surface imaging system. Low *et al* (2003) used a spirometer. Wolthaus *et al* (2005) used a thermometer placed in the breathing airflow in the patient's nostrils. Several authors have used strain gauges (Ohara *et al* 1989). Kubo and Hill (1996) made a comparison of the accuracy of various techniques, including a thermistor, a thermocouple, a strain gauge and a pneumotachograph. Movies were acquired at x-ray simulation using each method along with the reading from each candidate gating system. The temperature sensor and strain gauge were judged as the preferred systems based on characteristics such as reproducibility, accuracy, response speed and signal to noise ratio.

The respiratory signal used to acquire a 4D CT dataset may also be used to acquire a CT scan at a single breathing phase. The treatment would be planned and delivered at this

breathing phase. This would require both CT scanner and treatment room to have similar equipment for measuring the patient's breathing phase. Mageras and Yorke (2004) evaluated the use of respiratory gating for treatment in comparison with deep inspiration breath-hold (DIBH). They found that approximately half their patients could not comply with DIBH and hence there was the need to screen potential patients. The respiratory gating used the RPM system. The disadvantages of the DIBH approach were that it required active patient participation (hence the problem with patients being able to comply) and a breath hold is tolerable for a much shorter time than the several minutes taken by a radiotherapy fraction delivery or for a functional imaging procedure such as positron emission tomography. The use of treatment gating based on the external marker system was found still to require a level of patient effort and cooperation. Patients were coached verbally.

Patient coaching is often needed for both breath-hold and respiratory-gated approaches to CT (including 4D CT) and for treatments planned based on their use. This is because breathing is subject to variability, examples of which may be a variation in respiratory period or a drift in position (Dawson *et al* 2001, Seppenwoolde *et al* 2002, Mageras and Yorke 2004). This must be minimized to reduce artefacts in scanning and, in treatment, to avoid systematic errors introduced by differences between planning and treatment.

When gating CT acquisition (either to obtain a scan in a single position or a 4D set of scans), the choice of how to define the gating position is important. This is based on when one breathing cycle ends and the next starts. The potential for variability in the breathing cycle makes this an important choice. Two main approaches have been discussed in the literature, phase gating and amplitude gating (Vedam *et al* 2001, Shen *et al* 2003, Mageras and Yorke 2004). In amplitude gating, acquisition is triggered when the breathing trace is in a certain position and in phase gating triggering is based on when the breathing is at a given phase angle.

If a 4D CT dataset is acquired, it is often desirable to register the position of anatomy between the various phases. The advantages of doing this include calculation of the summed dose distribution over the whole breathing cycle (Lujan *et al* 1999, Coolens *et al* 2006, Rietzel *et al* 2006). Deformable motion models are generally necessary to achieve this, particularly as tumours of the lung and liver are soft tissues prone to deformation (see e.g. Balter *et al* 1996). The main approach adopted for the application to radiotherapy planning is the use of B-splines interpolants (Rueckert *et al* 1999, Hartkens *et al* 2002). Deformable motion models have been used for CT registration in a different context. Christensen *et al* (2001) presented an approach to combining dosimetry for external beam and intracavity brachytherapy. Three patients with locally advanced cervical cancer were treated with CT-compatible applicators and underwent five CT scans: before the start of external beam treatment and before and after two brachytherapy insertions. Datasets were registered using a viscous fluid flow model. Results were analysed in terms of a coincidence index (equivalent to the Jaccard index) and found the deformable registration to yield a range 90.6–100% compared with 5.2–72.2% without registration. A detailed review of these and other methods for deformable image registration may be found in Hill *et al* (2001).

The 4D CT approach generally involves establishing the mean trajectory of the target over several breathing cycles. This information is then used to plan the treatment strategy but may be subject to variability. Information on the variability has been sought in two ways: by the use of fluoroscopy (Chen *et al* 2001) and by data modelling (Land *et al* 2007). Low *et al* (2005) developed a five-dimension model of lung motion, as a combination of tidal volume and airflow components to describe the motion of a set of points as a function of breathing cycle. For the cases they studied, they were able to fit the motion of the points with an average discrepancy of 0.75 mm.

3.1.3. CT perfusion. The problems of target delineation may be reduced by the use of functional imaging, particularly in tumours expected to show an enhancement or detriment in uptake relative to adjacent normal tissues. This may be from a biological imaging modality such as PET (Nestle *et al* 2008) or a contrast agent in a modality such as CT or MRI. Contrast agents are starting to be used more frequently in CT scanning for radiotherapy planning, particularly for the head and neck region. There is the need to consider bulk correction to the CT numbers in the region of the contrast agent for accurate dose calculation purposes. The effect of contrast agent on dose calculation accuracy has been investigated. Choi *et al* (2006) measured the effect of intravenous contrast agent on IMRT dose planning for head and neck cancer. Fifteen patients each had two scans, one before and one after the contrast agent injection. Target volumes and organs at risk were contoured on the contrast-enhanced scan and IMRT plans created. The beams of the plan were copied onto the non-contrast enhanced scans and the dose distribution recalculated. Target dose values for the enhanced scans were found to be significantly lower than on the non-enhanced scans, but the dose differences were less than 1%. Dose to parotid glands and spinal cord were not found to be significantly different.

Perfusion measurement involves imaging a time sequence following the rapid intravenous bolus injection of a contrast agent (Axel 1980). A review of perfusion CT may be found in Miles and Griffiths (2003). One of the most significant studies of perfusion CT is the work of Hermans *et al* (1999, 2003) for head and neck cancer. In the first of their studies (1999) they investigated variability (both intra- and inter-patient and intra- and inter-observer) and the value of perfusion as a predictive factor of local failure after radiotherapy treatment for 41 patients. They found no significant difference between measurements performed by two independent observers. No correlation between the perfusion rate and tumour volume was found. No significant correlation between the perfusion rate and local control ($p = 0.19$) was found for the patient number studied. In the 2003 study, they evaluated perfusion as a predictive factor for local and regional failure in 105 head and neck patients. They stratified the patients according to the mean perfusion value and found those with the lower perfusion rates had a significantly higher local failure rate ($p < 0.05$). An example of a perfusion study is shown in figure 3 (Newbold *et al* 2005, Castellano 2006). Figure 3(a) shows a CT slice through the head and neck region, with various regions of interest identified, and figure 3(b) shows the temporal Hounsfield number change following administration of the iodine contrast agent (Newbold *et al* 2005, Castellano 2006).

Contrast enhanced CT has found particular use in brain imaging (e.g. Nabavi *et al* 1999, Hakime *et al* 2007). In radiotherapy, Sidhu *et al* (2004) considered delineation of brain metastases for radiosurgery treatment planning. They studied the effect of the timing between administration of the contrast agent and imaging on the measured volume of the lesion. Ten patients were given Omnipaque 300 contrast agent and scanned immediately following bolus injection and again with a delay of a median value of 65 min. Results showed an increase in the volume of the metastases in 86% of cases and the consequent choice of a larger collimator. In the case of two metastases, contrast was no longer visible in the delayed scan. No significant intra- or inter-observer variability was found. They concluded that the study showed the importance of the imaging protocol in the use of contrast enhanced CT.

3.1.4. Metal-induced artefacts. Metal body implants include artificial limbs, particularly hips (Coolens and Childs 2003), and fiducial markers implanted to aid target definition. By nature of their high attenuation of the kilovoltage x-ray source in the CT scanner, they produce artefacts that can cause problems in the use of CT data for radiotherapy planning. Firstly, the attenuation takes the raw signal outside the range for which the Hounsfield unit calibration is valid and hence affects dose calculation, and secondly streak artefacts from the implant obscure

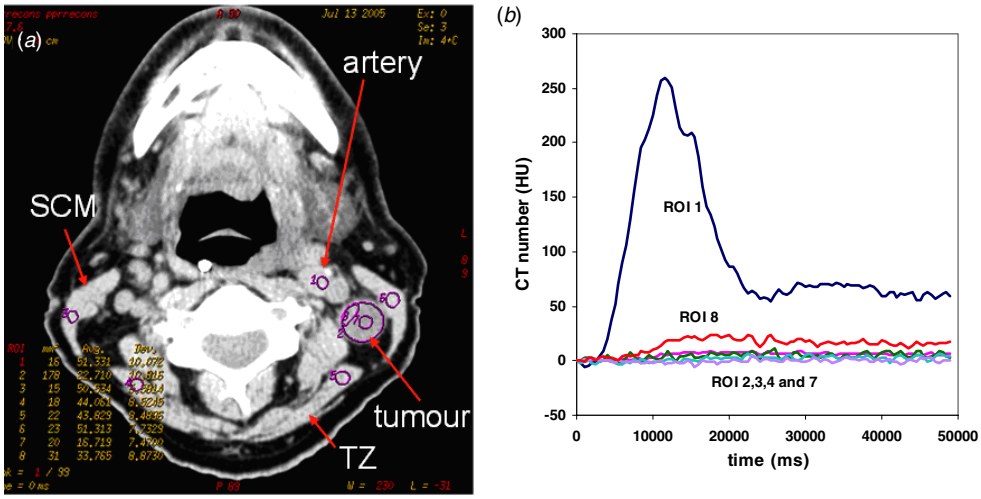

Figure 3. Illustration of a perfusion study for head and neck cancer. (a) A transaxial CT slice with various regions of interest (ROIs) marked. (b) Measured CT number as a function of time for a selection of the ROIs. The ROIs are arterial input (1), tumour (2, 7 and 8) sternocleidomastoid muscles (SCM) (3 and 6) and trapezius muscles (TZ) (4 and 5). Reproduced with kind permission from Castellano (2006).

useful soft-tissue structures that may help in target volume definition. Various approaches have been taken to reduce the effects of these artefacts. Examples include calibration of the CT scanner response by an electron density correction (Henson and Fox 1984) and the use of the stoichiometric method of Schneider as described above (Schneider *et al* 1996, Coolens and Childs 2003). Others have developed filters applied to the raw sinogram data or to the reconstructed data (Bal and Spies 2006). Figure 4 (Bal and Spies 2006) shows a CT scan of a prostate patient with implanted fiducial markers. The image is shown with and without a filter to reduce the severity of the streak artefacts. Jäkel *et al* have investigated the influence of metal artefacts in hadron therapy and showed that the distortion of CT number produced may significantly affect the calculated range of an ion beam (Jäkel and Reiss 2007).

3.1.5. CT number calibration. A CT scan is a map of attenuation coefficient at the energy of the scanner's x-ray tube, which may typically be a spectrum with maximum energy between 80 kVp and 150 kVp. Data are often displayed as Hounsfield units, with air assigned a value of 0 and water 1000 units. The dose calculation algorithms used in planning radiotherapy involve determining attenuation of the treatment beam or treatment radiation in the tissue of the phantom or patient, with correction for variations in tissue type (Cassell *et al* 1981). Algorithms currently used include Monte Carlo (Reynaert *et al* 2001, Verhaegen and Seuntjens 2003), collapsed cone kernels (Ahnesjö 1989) and pencil beam kernels (Gustafsson *et al* 1994). The variations in the tissue type are modelled with density corrections such as the equivalent path length model (O'Connor 1957, Milan and Bentley 1974, Sontag and Cunningham 1978, Ahnesjö and Aspradakis 1999). A lookup table is often used in the treatment planning system to scale data taken at the CT scanner energy to yield attenuation coefficient at the treatment energy (Henson and Fox 1984), which in external beam radiotherapy is often in the megavoltage range. The photoelectric effect is significant at the CT scan energies and negligible at the megavoltage energies with the Compton effect dominating.

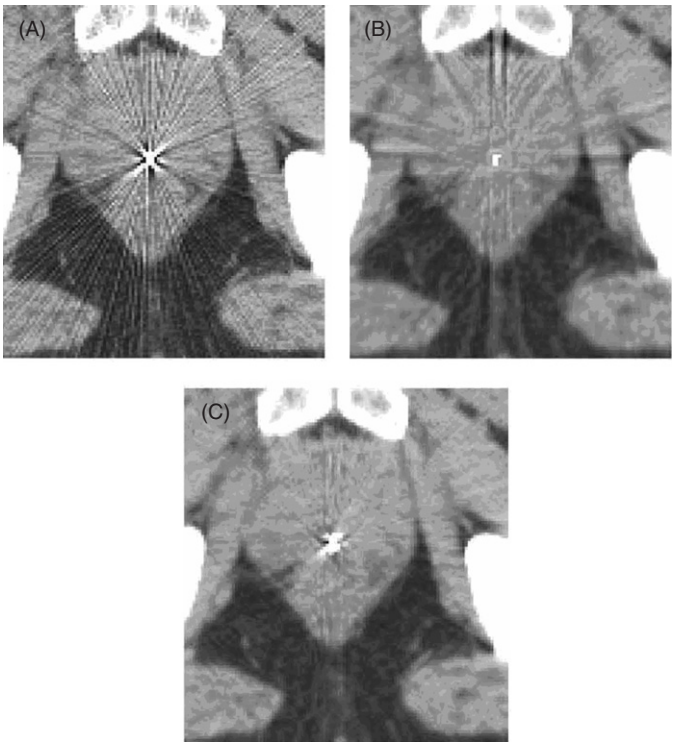

Figure 4. CT image of a prostate with an implanted fiducial marker showing typical metal artefacts (A). (B) and (C) The results of two methods of artefact correction. Reproduced with kind permission from Bal and Spies (2006).

The values for this lookup table are usually measured with a calibration phantom consisting of inserts of different densities. Often the lookup table is expressed as two or three linear regions (Seco and Evans 2006). The different contributions of photoelectric effect and Compton scattering in the two energy ranges is accounted for in this process. The first approaches to using kilovoltage energy CT data for megavoltage therapy planning were published in the late 1970s (Kijewski and Bjarngard 1978, Parker *et al* 1979). More recent work has refined this scaling, particularly in the context of accurate Monte Carlo treatment planning (Verhaegen and Devic 2005, Reynaert *et al* 2007). Refinements have included determination of the effects of variations in hydrogen content and extension to higher energies, where pair production becomes important (Seco and Evans 2006).

The conversion of Hounsfield numbers to stopping powers for hadron therapy has been discussed by several authors (Chen *et al* 1979, Mustafa and Jackson 1983, Schneider *et al* 1996, Jäkel *et al* 2001a, 2001b). Schneider *et al* used a stoichiometric approach to generate a table of proton stopping power as a function of electron density and Hounsfield number for a range of tissues of biological interest. Their results showed that changes in hydrogen content are also important for the calibration for hadron dose calculation.

3.1.6. Adaptive radiotherapy. The gating and 4D CT approaches described above are expected to be particularly valuable for sites where intra-fraction motion is important, such as the lung or liver. Other sites, such as the prostate or bladder, are expected to be more prone to

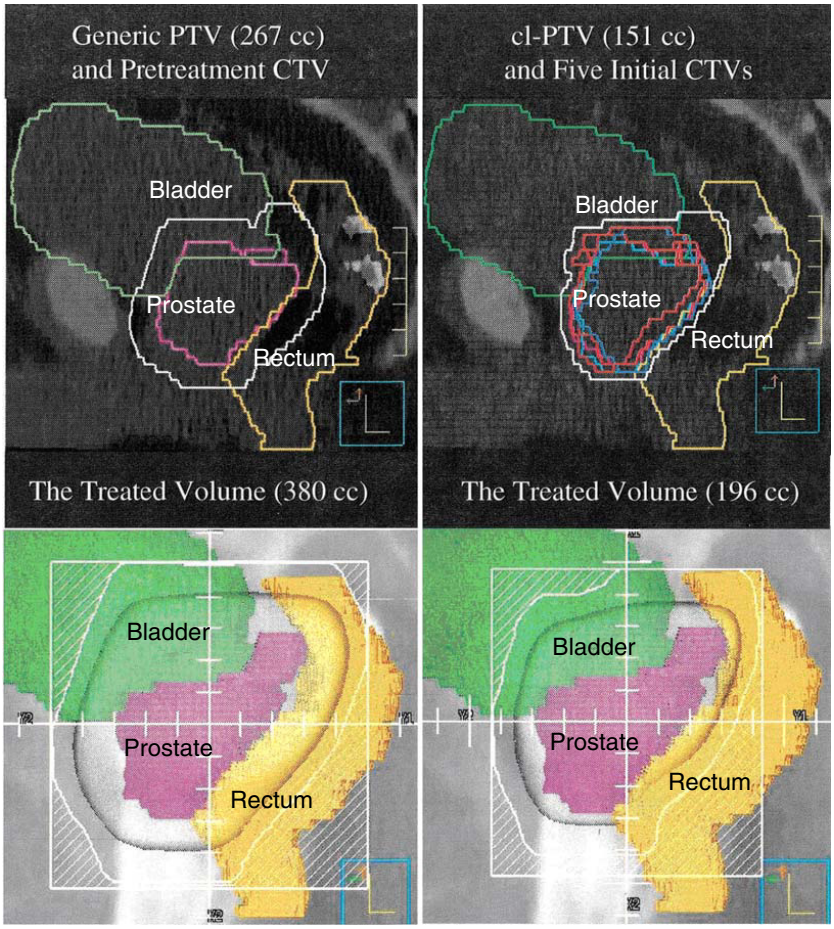

Figure 5. Illustration of the planning target volume (PTV, left) and confidence-limited planning target volume (cl-PTV, right) on the sagittal CT scan of a patient, and the corresponding treated volume (shaded area) on the beam's eye view digitally reconstructed radiograph. Reproduced with kind permission from Martinez *et al* (2001).

inter-fraction or day-to-day variation. Again a single scan constitutes a single snapshot image which may not be indicative of the anatomy throughout the patient's treatment.

Yan and colleagues (Yan *et al* 1998, Martinez *et al* 2001) have proposed a method called adaptive radiotherapy (ART) which seeks to ameliorate this problem by obtaining a set of CT scans of the patient on different days at the start of treatment and designing the target volume using the extra information from this set of scans and electronic portal imaging (EPI) on each treatment day. The method was applied to prostate cancer patients. In the report by Martinez, 150 patients had an initial CT scan from which a treatment plan was made. On the first 4 days of treatment, CT scans and EPI data were obtained. These were used to generate a confidence limited planning target volume (cl-PTV) (see figure 5, Martinez *et al* 2001). The CT scans were first registered to correct for day-to-day positional variations using bony anatomy. To generate the cl-PTV, the convex hull of the extent of the PTV was then constructed. The effects of better definition of PTV were modelled to determine the dose escalation achievable whilst satisfying dose constraints specified for the rectal wall. The conclusion was that ART allowed a 5% dose escalation for conformal radiotherapy and 7.5% escalation for IMRT.

Pos *et al* (2006) have evaluated ART for bladder treatment. For a group of 21 patients, five daily CT scans were acquired immediately before or after irradiation (randomly selected to avoid bias), during the first week of treatment and used to construct the cl-PTV (referred to as PTV_{ART}). A treatment plan based on this was used from the third week and further CT scans were taken to measure the accuracy of ART. The results were quantified in terms of the treatment volume reduction achievable with ART and showed a 40% saving compared with conventional.

3.2. Magnetic resonance imaging

Magnetic resonance imaging (MRI) has become an important imaging modality in radiotherapy planning, complementing the use of CT. It provides several advantages over CT, including improved soft-tissue visualization and hence better target delineation; it is fundamentally 3D (rather than a stack of 2D slices as in CT), and novel techniques are available such as cine MR and magnetic resonance spectroscopy (MRS). Disadvantages include the lack of an attenuation correction map for dose planning, geometric distortion and cost. MRS is a biological imaging modality and so not within the remit of this review. A detailed review of MRS in radiotherapy treatment planning may be found in Payne and Leach (2006).

We now consider the various aspects of MRI in radiotherapy treatment planning. Firstly, we consider target delineation using MRI and comparison of MRI outlining with CT outlining, then we consider the use of contrast enhanced MRI to aid target definition, then methods for correction of spatial distortion in MRI are presented and finally, the use of MRI for dose calculation is reviewed.

3.2.1. Target delineation. Several studies have evaluated MRI for target volume definition and often the results have been expressed in terms of comparison between MRI and CT volumes and their treatment planning consequences.

For the prostate, MRI and CT were compared by Roach *et al* (1996). Ten patients were scanned with T1-weighted MRI and CT (without the use of contrast agent). The bony anatomy on the images was matched and the measured prostate volumes (excluding seminal vesicles) compared. Retrograde urethrograms were used to assist with definition of the inferior border of the prostate (Roach *et al* 1993). The mean prostate volume was found to be 32% larger on average (range 5–63%) for CT. Discrepancies in volume definition were associated with four regions in the prostate: the posterior part, the posterior–inferior–apical part, difference in apex position between the urethrogram and MRI, and regions corresponding to the neurovascular bundle. They discussed using contrast enhancement in the CT scan as an alternative. Rasch *et al* (1999) compared MRI and CT for delineation of prostate and seminal vesicles in 18 patients. Proton density MRI scans were taken in axial, coronal and sagittal planes and compared with CT. As with Roach's study, the CT volumes were found to be larger, in this case by 43% ($p < 0.005$) for axial scanning. Axial MRI volumes were, on average, found to be 1.09 and 1.19 times the coronal and sagittal volumes, respectively. Systematic differences between the positions of the apex of the prostate and seminal vesicles were evaluated, with both found to be 6–7 mm closer to the centre of the prostate on the axial MRI scans, with coronal MRI scans agreeing to be within 1.5–3 mm on average. Variability between three observers was measured and found to be a smaller factor than choice of scan modality. They recommended that axial MR should be used for delineation, with a combination of axial and coronal scans in case of doubt, and the CT scan to be used for treatment plan dose calculation. Debois *et al* (1999) found broadly similar results using T2-weighted axial and coronal MRI data, with the average CT volume 46% bigger than on axial MRI for nine patients, plus one

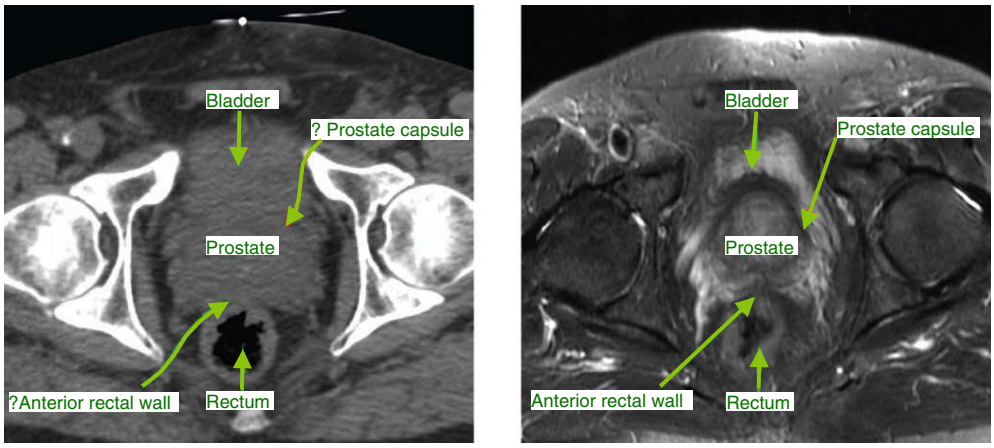

Figure 6. CT slice through a prostate (a) and the corresponding MR scan (b). Reproduced with kind permission from Khoo and Joon (2006).

patient showing a larger volume on MRI than on CT. Inter-observer variability in the location of the apex was measured for three observers and found to be best for coronal MRI and worst for CT. The effect on planned dose to rectum was compared for the modalities and it was found that the volume of rectum on the MRI scan receiving more than 80% of the prescribed dose was reduced by 23.8% on average compared with CT organ delineation. Jackson *et al* (2007) found a 14% bigger prostate volume for CT (11 patients) and that the planned percentage of rectum treated to doses above 45 Gy (prescribed treatment dose 70 Gy) was significantly lower for T2-weighted MRI compared to CT. Khoo and Joon (2006) reviewed new developments in MRI for target volume delineation. Figure 6 (from Khoo and Joon 2006) shows a CT slice through a patient's prostate and the corresponding T2-weighted MRI slice, revealing better visualization of organ boundaries.

MRI has the advantage that rapid images may be acquired without the dose associated with cine CT. An example of the use of this in radiotherapy is the evaluation of rectal distension and rectal movement on prostate position using cine MRI (Padhani *et al* 1999). Fifty-five patients were scanned axially using a T1-weighted spoiled gradient-echo sequence and a T1-weighted turbo-FLASH sequence every 10 s for 7 min. Twenty-four patients received bowel relaxants before imaging. Rectal movements were seen in 51% patients overall. A smaller percentage of those receiving relaxants showed movement, but the result was not statistically significant. Incidence of rectal movement correlated with degree of rectal distension, but the magnitude of that movement did not. The rectal movements correlated well with prostate movement. Prostate movements in the anterior–posterior direction were seen in 29% patients and in 16% of patients the movement was greater than 5 mm. The conclusions of the study were that rectal movements result in displacements that are significant in magnitude for radiotherapy planning over a time period similar to the delivery of a radiotherapy fraction.

Ten Haken *et al* (1992) evaluated MRI delineation of brain tumours in 15 patients (5 with low-grade astrocytomas and 10 with higher grade glial tumours). The datasets used consisted of CT scans with iodinated intravenous contrast and a variety of MRI scans: axial T2 weighted, axial T1 weighted and coronal T1 weighted. The T1-weighted scans were taken with gadolinium contrast. Two components to the target volume were defined on each imaging modality: a microscopic volume defined by oedema on CT and increased T2 signal on MRI, and a macroscopic/boost volume defined by contrast enhancement on CT and T1-weighted

MRI. MRI defined volumes (both microscopic and macroscopic) were larger than for CT. The composite volume, defined as the sum of CT and MRI, had just 50–55% overlap between CT and MRI. The PTV (made by expanding the microscopic volume by 2 cm in all direction and the macroscopic volume by 1 cm) showed greater overlap with 79% and 69% respectively. Weltens *et al* (2001) studies inter-observer variability in brain tumour definition, combining CT and MRI for five patients with inoperable supratentorial tumours. Nine physicians participated in the study. A larger variation in outlining was found. The ratio of largest to smallest CT GTV volume outlined was between 1.7 and 2.8. Use of MRI plus CT still produced a large variation in the volume ratio—between 1.5 and 2.4. The volumes delineated on the combined scan data were on average 17% higher than on CT alone.

Other treatment sites where MRI target definition has been evaluated include base of skull meningiomas (Khoo *et al* 2000), central nervous system (Aoyama *et al* 2001) and liver (Teefey *et al* 2003).

3.2.2. MRI contrast enhanced, perfusion and diffusion imaging. MRI perfusion and diffusion imaging have been evaluated for imaging cancer. A review of the underlying physical principles may be found in Thomas *et al* (2000).

Rouviere *et al* (2004) evaluated gadolinium dynamic contrast enhanced (DCE) MRI versus T2-weighted MRI for localization of intraprostatic lesions in 22 patients. They correlated their findings with biopsy results and measured variability between three observers. The DCE imaging produced better agreement with biopsy and better inter-observer agreement than the T2-weighted images. Storaas *et al* (2004) also evaluated DCE MRI for prostate localization. Twenty-eight patients were imaged with gadolinium DCE T1-weighted 3D echo planar imaging and a T2-weighted turbo spin echo (TSE) sequence. Comparison was also made with histology from resected specimens. No statistically significant improvement in localization of prostate or seminal vesicles was found by adding the DCE information, and they concluded that the DCE sequence did not improve tumour localization compared to the T2-weighted sequence.

Sumi *et al* (2003) evaluated the use of diffusion-weighted MRI to detect metastatic cervical lymph nodes in head and neck cancer patients. Diffusion-weighted echo planar imaging and T1- and T2-weighted MRI sequences were performed on a set of patients' lymph nodes. The results were correlated with histology. The apparent diffusion coefficient (ADC) was found to be significantly greater in metastatic lymph nodes than in benign lymphadenopathy ($P < 0.01$) with nodal lymphomas having the lowest ADC values. Applying an ADC criterion for the detection of metastatic nodes yielded a negative predictive value of 71% and a positive predictive value of 93%. A fuller review of diffusion MRI to assess cancer therapeutic efficiency may be found in Chenevert *et al* (2000).

MRI perfusion has been used to study blood flow in brain tumours (Cha *et al* 2002, Keston *et al* 2003). Wenz *et al* (1996) compared perfusion in low-grade astrocytomas and normal brain tissue before and after radiotherapy. Results showed a significant reduction in blood volume within the tumours after irradiation, with an insignificant reduction for grey and white matter outside the target volume. By comparison a significant reduction in blood volume for grey and white matter was observed after whole-brain irradiation, suggesting perfusion MRI may be used to monitor tumour response and normal tissue effects in radiotherapy.

3.2.3. Image distortion correction. Imaging data for radiotherapy treatment planning should have good geometric accuracy, as distortion will contribute to systematic errors in the positioning of tissues and potentially dose calculation errors. It is well known that MRI

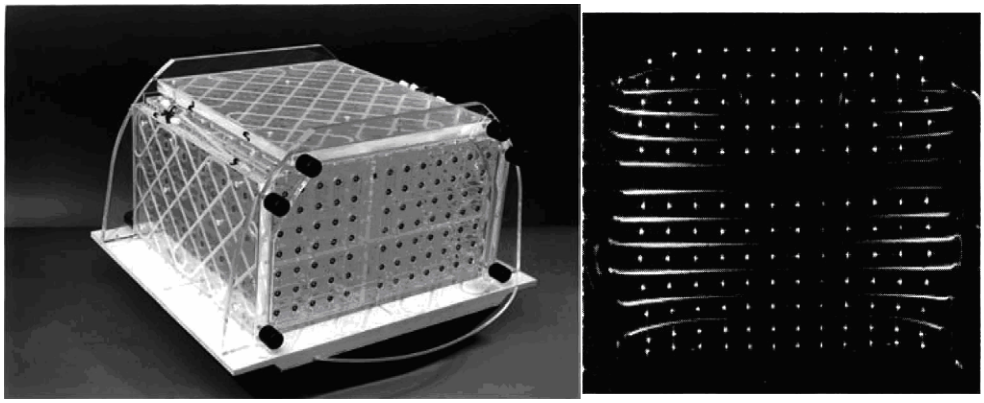

Figure 7. Linearity test phantom (left) and an uncorrected coronal MRI scan acquired from this phantom (right). The spots within the image arise from a regular lattice of water-filled marker tubes. Image distortion is evident from the irregular positioning of the spots and warping out of the plane of the image is seen in the appearance and disappearance of the straight marker tubes lying in the imaging plane. This image was acquired at the periphery of the imaging volume and hence distortion is particularly severe in this case. Reproduced with kind permission from Tanner *et al* (2000).

systems suffer from geometric distortions due to issues such as variations in magnetic field strength, gradient field non-linearity and susceptibility effects. Distortions have been shown to range from typically 0.2 to 5 mm as the distance from the centre of the magnetic field increases from 5 to 10 cm Prott *et al* (2000). For these reasons there is much interest in quantifying this distortion, establishing its effect on treatment dosimetric accuracy and developing methods to correct for it.

Kooy *et al* (1994) demonstrated the use of chamfer matching to fuse CT and MRI for radiosurgery planning. They presented two cases, an acoustic neurinoma and a pilocytic astrocytoma. They concluded that MRI is necessary in stereotactic therapy, with superior diagnostic quality, but with poor geometric fidelity. Prott *et al* (2000) investigated the effects of MRI distortion on radiotherapy treatment planning. They investigated 27 MRI units. The distortions were found to cause small variations in maximum dose ($\pm 0.5\%$). Changes in the 95% isodose volume were seen (25% cases showed an increase and 60% a decrease). Organ at risk dose variations were found to be comparable to those in the PTV.

Several groups have evaluated methods of distortion correction for treatment planning. Tanner *et al* (2000) described the removal of MRI system distortions using a geometric phantom consisting of orthogonal arrays of water-filled polymethylmethacrylate tubes. Figure 7 shows an uncorrected coronal image of the phantom. Results showed that distortions were over 10 mm for larger distances off axis. Reproducibility of the measurements was of order 0.1 mm indicating the accuracy expected from such a calibration procedure. Most current clinical MRI systems have 1.5 T field strength. Petersch *et al* (2004) evaluated distortion in a 0.2 T system and its effects on treatment planning. They found that using the phantom calibration method to remove system effects reduced maximum distortion from 28.0 to 13.7 mm with mean distortion reduced from 2.2 to 0.6 mm and 95% of points with a distortion of less than 1.5 mm. Object-induced distortions were also investigated and found to be a second-order effect. Wang *et al* (2004a, 2004b, 2004c) studied geometric distortion in several models of MRI systems. They measured distortion using a purpose built phantom consisting of a 3D grid of crosses. They found similar results to other investigators, with maximum distortion errors between 10 and 25 mm and corrected images accurate to better than 0.8 mm.

3.2.4. Treatment planning using MRI alone. In treatment sites without significant tissue inhomogeneity, there is the potential to use MRI alone for treatment planning, with a bulk density correction applied for dose calculation in the absence of an electron density map from CT. Beavis *et al* (1998) investigated MRI for planning brain treatments. MRI planning has also been studied for prostate treatment (Lee *et al* 2003, Petersch *et al* 2004). For a 1.5 T system, Lee showed distortions of 2 mm in the vicinity of the prostate for FLASH 3D T1-weighted images and that the use of bulk density assignment to water and bone produced treatment plans with similar percentage volumes of rectum receiving greater than 50% dose to CT for conformal treatment. The plan to extend this work to T2-weighted imaging, with greater contrast, was discussed. Petersch investigated the use of the 0.2 T resistive MRI system discussed above. Dose calculations, with all tissues taken as water equivalent, showed agreement with CT of 1% in the dose at the normalization point in four out of five cases studied.

3.3. Ultrasound

Ultrasound has been used to assist target definition in treatment planning, particularly in the absence of CT data. Some of these applications are being replaced by CT and MRI, but the development of new technology, including 3D scanning (Treece *et al* 2003) and tissue characterization imaging (Burnside *et al* 2007), means that ultrasound has an important contribution to anatomical imaging for radiotherapy planning. Ultrasound has been used in several target localization studies for post-lumpectomy breast radiotherapy. DeBiose *et al* (1997) demonstrated localization of the lumpectomy cavity for interstitial brachytherapy; Helyer *et al* (1999) investigated the determination of the depth of the tumour bed and consequent selection of electron boost energy and Coles *et al* (2007) made a comparison of 2D and 3D ultrasound with CT for localization of the tumour bed. They concluded that co-registration of 3D ultrasound with planning CT data can be used to yield additional information on the size and position of the tumour bed to be incorporated into the planning volumes. Featherstone *et al* (1999) used ultrasound to localize the ovaries for radiation-induced ovarian ablation as part of breast cancer treatment. Orecchia *et al* (2007) used ultrasound to measure the treatment of prostate cancer with intraoperative radiotherapy (IORT). Eleven patients were treatment with pelvic lymphadenectomy, prostate IORT (with an electron beam from a mobile linear accelerator) and radical retropubic prostatectomy. Prostate thickness and depth of rectum were measured with ultrasound and used to quantify the dose distribution to the prostate and rectum.

Real-time transrectal ultrasound (TRUS) has been used to enable image-guided source implantation in brachytherapy treatment of localized prostate cancer (Blasko *et al* 1993, 1995, Hoskin and Bownes 2006, Lawton *et al* 2007). Blasko *et al* presented a method for transperineal permanent implantation of ^{125}I and ^{103}Pd seeds. In their method, they took a set of transverse ultrasound images covering the prostate volume and determined the optimum seed distribution. The seeds were then implanted under biplanar ultrasound guidance to enable the operator to visualize the needle placement in both transverse and sagittal planes and to see the prostate movement. Post-implantation, a CT scan was taken to enable dose calculation. They contrasted their method with the older retropubic approach and concluded that better dose homogeneity, greater reproducibility and a larger treatment volume are achievable with the new method. Four hundred and sixty-nine patients were treated with the image-guided technique. Follow-up for a median time of 37 months showed favourable prostate-specific antigen (PSA) levels. Lawton *et al* (2007) recently presented results of a multicentre, phase 2 study, in which 95 patients were treated with the ultrasound-guided transperineal method.

Patients were followed up for a mean time of 5.3 years. Survival at 5 years was 96.7%. Six per cent had biochemical failure. They concluded that the outcome results were comparable to other brachytherapy data and the results of surgery and external beam radiotherapy.

Ultrasound guidance has also been used to aid source implantation in brachytherapy of gynaecological malignancies. Stock *et al* (1997) presented the use of TRUS image-guided for a series of cases (4 cervical, 2 endometrial and 1 vaginal). Sahinler *et al* (2004) demonstrated the use of transvaginal ultrasound guidance for the placement of tandem applicators for cervical cancer treatment. The ultrasound scan was used to judge the likely difficulty of applicator insertion and found to have a good predictive value.

4. Anatomical imaging in verification

Anatomical imaging for treatment verification is an essential part of the radiotherapy process. Recent years have seen significant technological development of a number of complementary approaches to this problem. The essential goal of treatment verification is to minimize and quantify any differences between the treatment as planned and delivered. Quantification of differences is in terms of the geometrical errors discussed above and ultimately the dose distribution and predicted impact on treatment outcome. The use of imaging of soft tissue for verification, particularly in external beam radiotherapy, is often referred to as image-guided radiotherapy (IGRT) verification (Jaffray 2007) or the target of the day (Mackie *et al* 1999). The term IGRT has also been used in terms of planning using functional imaging (Chao *et al* 2001) and using imaging dynamically in a procedure (Zamorano *et al* 1987) such as the TRUS methods discussed in the previous section.

Imaging taken as part of verification may also be used in an adaptive radiotherapy (ART) model. Whereas the ART approach discussed in section 3.1.6 involved building a model of target motion prior to treatment and planning based on this model, the use of verification image ART involves determining the treated dose distribution and correcting for differences compared to the planned distribution (De la Zerda *et al* 2007, Webb 2008).

A wide variety of techniques have been applied to IGRT, including the following:

(1) megavoltage x-ray electronic portal imaging (EPI)
(2) kilovoltage x-ray portal imaging
(3) kilovoltage CT (most commonly conebeam, but also CT on rails in the treatment room)
(4) megavoltage CT (including tomotherapy)
(5) electromagnetic marker tracking
(6) ultrasound
(7) optical methods.

The portal imaging methods, 1 and 2, being projection based, are good for imaging a bony structure. In order to determine soft-tissue positioning, they are generally used in conjunction with surrogate, fiducial markers. Thus they are invasive, but have the potential to be used for tracking intra-fraction motion if sufficiently rapid data can be acquired. The CT methods, 3 and 4, involve pre-treatment scanning, allow soft-tissue visualization, facilitate adaptive radiotherapy and provide information similar to the data used to plan the treatment. They are useful for determining inter-fraction variations. The first four methods all entail extra dose to non-target tissues in the patient (except the use of megavoltage portal imaging of the delivered beam). Electromagnetic tracking, ultrasound and optical imaging entail no extra dose. Electromagnetic marker tracking provides a real-time 3D movement map of implanted fiducials. Ultrasound allows soft-tissue visualization but requires a skilled operator, scanner set-up and may be prone to tissue distortion from the probe pressure.

Table 1. Summary of properties of imaging methods used for image-guided radiotherapy. MV denotes megavoltage and kV kilovoltage.

Imaging method	Dose required	Soft-tissue visualization	Pros	Cons
Megavoltage portal	2–10 cGy (may be treatment beam)	Surrogate markers	Motion tracking feasible Treatment dosimetry	MV image quality Bony anatomy only Need for markers
Kilovoltage portal	0.2–8 cGy (Shirato *et al* 2004)	Surrogate markers	Motion tracking Better quality than MV	Skin dose for tracking Extra radiation source needed Need for markers
Kilovoltage CT	1–3 cGy (Islam *et al* 2006)	Yes	Soft-tissue visualization Adaptive treatment Intrafraction motion Dosimetry feasible	Conebeam quality versus conventional CT Pre-treatment scan time Extra radiation source
Megavoltage CT	1–15 cGy (Pouliot *et al* 2005, Meeks *et al* 2005)	Yes	Soft-tissue visualization Adaptive treatment Intrafraction motion Dosimetry attenuation coefficient map	May require skilled interpretation Pre-treatment scan time Lower quality than kV Larger dose than kV
Electromagnetic marker tracking	None	Surrogate markers	Motion tracking Zero dose	Need for markers No internal anatomy
Ultrasound	None	Yes	Soft tissue Zero dose Off-line motion tracking	Skilled interpretation needed Scanner set-up Tissue distortion
Optical	None	No	Zero dose Zero invasiveness Surface motion tracking	No internal anatomy Combine with x-rays

Optical systems are completely non-contact, but only allow surface imaging and hence must be used with imaging of internal anatomy and/or a model of the relationship between motion of internal and external anatomy. The utility of ultrasound and optical imaging are treatment site dependent. Megavoltage portal imaging and the two CT methods may be used to provide treatment dosimetry estimation. A summary of some of the properties of these imaging methods is presented in table 1. Newer verification techniques are being developed including the incorporation of an MRI scanner into the external-beam treatment machine (Raaymakers *et al* 2004).

4.1. Megavoltage portal imaging

Several excellent reviews of megavoltage EPI have been written (Boyer *et al* 1992, Herman *et al* 2001, Langmack 2001, Antonuk 2002, Herman 2005, Kirby and Glendinning 2006). EPI has the attraction that it images the actually treatment beam (hence may involve no extra dose) and provides some information on internal anatomy. The fact that it provides projection images using higher x-ray energy limits the quality of the information available, however. Several imaging technologies have been applied to EPI (see the reviews of Boyer *et al* and Antonuk), but the majority of currently used systems are based on amorphous silicon flat panel imagers (FPIs) (Antonuk *et al* 1992), with one system based on a CCD camera (De Boer *et al* 2000). FPIs are used for many of the alternative x-ray verification systems including kilovoltage portal imaging and conebeam CT (CBCT).

In terms of anatomical imaging, the information most commonly available is the position of bony anatomy relative to the radiation field edge. Hurkmans *et al* (2001) made a thorough

review of the literature on the measurement of random and systematic inter-fraction treatment errors for a variety of treatment sites: head and neck, prostate, pelvis, lung and breast. Soft-tissue imaging has been achieved using implanted fiducial markers as a surrogate (Vigneault *et al* 1997, Nederveen *et al* 2002, 2003, Ford *et al* 2002a, Aubin *et al* 2003, Chen *et al* 2007). Nederveen *et al* (2003) compared the measurement of positional errors based on bony anatomy with the use of fiducial markers. They evaluated 2025 portal images in comparison with CT for 23 patients. Standard deviations in systematic marker position deviations of 2.4–4.4 mm were found. An offline correction protocol (Bel *et al* 1993) reduced this to under 1 mm. The use of bony anatomy in the correction protocol, in place of the fiducials, reduced the set-up error by 50% in two directions, but no reduction was found in the cranio-caudal direction. This study showed the value of the fiducial markers and that large set-up margins may still be needed if basing corrections on bony anatomy. McDermott *et al* (2006) showed how changes in anatomy could be determined using different images. Examples presented include progressive changes in lung cancer patients in response to irradiation.

Other applications of EPI include dosimetry, which may be empirical measurement (Hansen *et al* 1996, Pasma *et al* 1999, McDermott *et al* 2004, Greer 2005, Winkler *et al* 2005, Wendling *et al* 2006) or model based (Spies *et al* 2000, McCurdy *et al* 2001, Spezi and Lewis 2002, Siebers *et al* 2004, Parent *et al* 2006), and IMRT verification (Warkentin *et al* 2003, Van Esch *et al* 2004, Wendling *et al* 2006). Commercially available detectors have low quantum efficiency (QE) at 1–2%. Several groups are developing higher efficiency systems using approaches such as thick scintillators or a structured high-density material (Mosleh-Shirazi *et al* 1998a, Pang and Rowland 2002, Sawant *et al* 2002, 2005, Evans *et al* 2006b) to increase the efficiency by an order of magnitude, with the challenge of maintaining spatial resolution.

4.2. Kilovoltage portal imaging

Kilovoltage projection imaging has long been used in radiotherapy in the x-ray treatment simulator. With the advent of CT simulation (see e.g. Nishidai *et al* 1990) the role of the conventional simulator has changed and several groups have used simulator fluoroscopy to measure intra-fraction breathing motion. Malone *et al* (2000) measured prostate motion using fiducial markers and Poggi *et al* (2003) evaluated marker migration. Chen *et al* (2001) and Sixel *et al* (2003) evaluated tumour motion in lung patients. This was carried out without markers, based on image intensity. The purpose of such studies was to determine the margins needed to account for intra-fraction motion.

By incorporating diagnostic-energy x-ray imaging into the treatment room, it is possible to acquire kV portal images for treatment verification. As early as 1985 a diagnostic x-ray set was mounted on a treatment linac (Biggs *et al* 1985). Several authors have compared MV and kV portal imaging for set-up correction (Jaffray *et al* 1995, Pisani *et al* 2000). The early studies were with film or camera-based systems. These have been replaced by the FPI systems. Manufacturers are starting to provide kV imaging systems on the treatment unit to enable kV projection and CBCT imaging (Jaffray 2005, Yoo *et al* 2006). These are generally mounted at right angles to the treatment beam.

Systems with one kV imager provide 2D information. The combination with orthogonal MV imaging can provide 3D information. A favoured approach is to incorporate at least two kV systems to enable stereoscopic 3D imaging. Up to four systems are installed to enable imaging at gantry angles which might obscure one of the systems. These systems are often

used in conjunction with implanted fiducial markers to enable tracking of mobile tumours, such as in the lung or liver.

The first example of this approach was in a robotic radiosurgery system (Adler *et al* 1999, Murphy *et al* 2003). This used two orthogonal, floor-mounted FPI detectors and ceiling mounted x-ray sets. Yin *et al* (2002) reported the use of a similar system for intensity modulated radiosurgery of spinal tumours. Massachusetts General Hospital has also developed a system with two x-ray tubes mounted 45° from the treatment head (Berbeco *et al* 2004). These systems also use infrared tracking to complement the x-ray systems and allow tracking between x-ray verification images, thus reducing x-ray dose (Jiang 2006, Jin *et al* 2007).

The group of Shirato (Shirato *et al* 2000a, 2000b, 2004b, 2006, Shimizu *et al* 2001, Seppenwoolde *et al* 2002) developed a system with four floor-mounted x-ray tubes with ceiling-mounted x-ray image intensifiers that imaged at 30 frames s^{-1}. A 2 mm gold fiducial marker implanted in the body was imaged using x-ray energies of 50–120 kVp. The dosimetric consequences of using this system in fluoroscopic mode for real-time tumour tracking were evaluated. The surface dose was found to be between 28 and 980 mGy h^{-1}, depending on kVp and x-ray pulse width (Shirato *et al* 2004a).

4.3. Kilovoltage CT

Kilovoltage CT in the treatment room provides 3D anatomical information including soft tissue and thus provides advantages over the portal imaging methods described above. However the scan is generally obtained prior to therapy and hence has limited information on intra-fraction variations. Two approaches have been developed: the incorporation of a diagnostic CT scanner in the treatment room and the attachment of a kilovoltage source and FPI on the treatment linac and scanning in conebeam geometry (Feldkamp *et al* 1984).

The requirements of CT in verification are similar to those in treatment planning (section 3.1). The issues of target delineation are similar, as are the problems with imaging the moving patient and artefacts caused by metal implants. There is also interest in the use of such systems for dose planning, making the need for accurate CT number calibration a challenge.

The use of diagnostic scanners in the treatment room is achieved by moving the treatment couch between the treatment machine and the CT scanner and is often referred to as CT on rails. Court *et al* (2003) evaluate the positional accuracy of such a system in terms of the component errors introduced by the need to move the couch. They evaluated two positioning protocols: one relying on the mechanical integrity of the system and the other one using radio-opaque markers in the treatment couch. The first had positional accuracy of 0.6–0.7 mm and the second better than 0.5 mm. This system is further described in Ma and Paskalev (2006). Kuriyama *et al* (2003) evaluated an alternative system and found comparable accuracy of 0.4 mm.

The duel-energy imaging system of Jaffray discussed above was used to take CBCT scans on the treatment unit, using an x-ray tube at 90° to the treatment beam and a camera-based imager initially (Jaffray *et al* 1999) and a FPI ultimately (Jaffray and Siewerdsen 2000, Jaffray *et al* 2002). Ding *et al* (2007) describe a similar system. Létourneau *et al* (2005) demonstrated the use off the conebeam geometry to produce images with high spatial resolution in all three directions with a sagittal slice through a prostate patient showing good definition of bladder, prostate, seminal vesicles, rectum and sigmoid colon (see figure 8). One of the potential disadvantages of the conebeam geometry is the larger amount of scattered x-rays, which may increase noise in the reconstructed images and hence reduce detectability of low contrast objects (Endo *et al* 2001). In addition it may be desirable to use the images for dosimetric verification, either by inputting the images to the dose calculation algorithm on the treatment

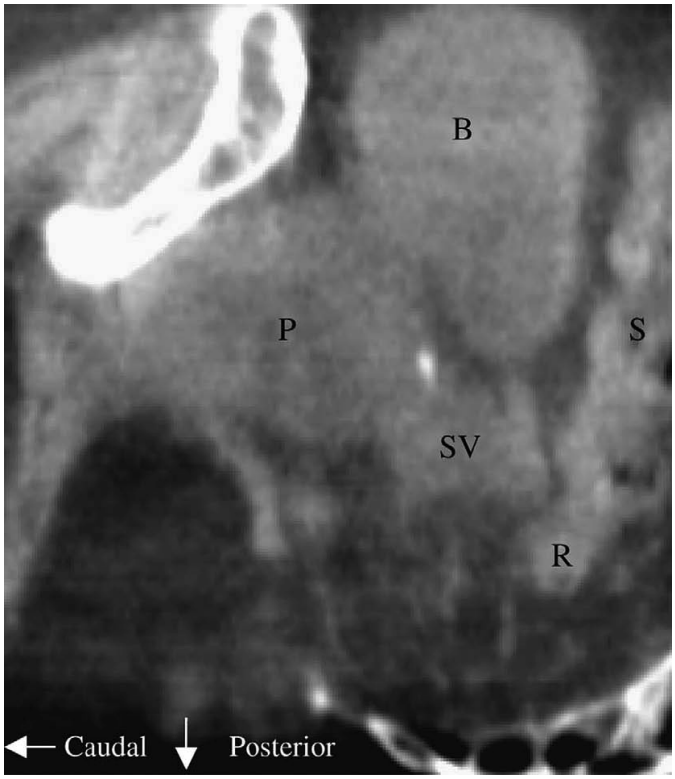

Figure 8. Sagittal conebeam CT slice through a prostate patient. The image shows various soft-tissue features: bladder (B), prostate (P), seminar vesicles (SV), rectum (R) and sigmoid colon (S). Reproduced with kind permission from Létourneau *et al* (2005).

planning system or using a transit dosimetry approach (Hansen *et al* 1996, McNutt *et al* 1996). The scattered radiation may affect the Hounsfield number calibration, thus introducing uncertainty to the dose calculation (Malušek *et al* 2005). Siewerdsen *et al* (2004) demonstrated the use of anti-scatter grids and Jarry *et al* (2006) demonstrated the use of a Monte Carlo based correction method, which improved calibration for a variety of phantom materials. Yoo and Yin (2006) evaluated the dose planning accuracy of uncorrected images and showed that in most cases the error was below 1%, with 3% error in an inhomogeneous phantom. Patient doses have been evaluated and found to be of order 1–3 cGy (Islam *et al* 2006, Amer *et al* 2007). Solutions to problems identified in conventional CT have also been developed for CBCT, including metal artefact reduction (Zhang *et al* 2007) and correction for respiratory motion (Sonke *et al* 2005, Schreibmann *et al* 2006). Several papers have demonstrated clinical applications of CBCT (e.g. Sykes *et al* 2005, Henry *et al* 2006, White *et al* 2007, Létourneau *et al* 2007).

4.4. Megavoltage CT

Megavoltage CT (MVCT) uses the treatment beam to make a scan and hence provides an alternative method of treatment-time CT without the need for additional x-ray sources or detectors. The first implementations used a single row of high QE elements comprised of

photo-diodes and scintillators, scanned in third generation geometry (Simpson *et al* 1982, Swindell 1983, Brahme *et al* 1987, Nagakawa *et al* 1991, Lewis *et al* 1992). Later systems used conebeam geometry, either based on a high QE scintillator array coupled to a camera (Mosleh-Shirazi *et al* 1998a, 1998b) or an FPI (Hesse *et al* 1998, Ford *et al* 2002b, Sillanpaa *et al* 2005, Pouliot *et al* 2005). One system has combined high QE with the use of an FPI (Seppi *et al* 2003). Tomotherapy uses MVCT for verification (Mackie *et al* 1999, Ruchala *et al* 1999, Forrest *et al* 2004, Meeks *et al* 2005). The detector used is a high-pressure xenon ionization chamber.

The limitations of MVCT in comparison with diagnostic energy CT arise from the lower quantum efficiency of a detector at the megavoltage energy and the lower intrinsic contrast between the various tissues. However, trade-offs may be made in terms of quantities such as the spatial resolution required to limit the dose needed (Simpson *et al* 1982). Advantages of MVCT over conventional CT include the reduction of artefacts due to high Z materials such as dental fillings (see section 3.1.4) (Pouliot *et al* 2005, Lu *et al* 2006a). Also as the images are attenuation maps in the treatment beam, MVCT may readily be used for treatment planning dose calculation and dose verification without the need for a conversion table as in conventional CT (see section 3.1.5) (Simpson *et al* 1982, Aoki *et al* 1990, Kapatoes *et al* 2001, Langen *et al* 2005, Morin *et al* 2007). Yin *et al* (2005) combined projections from kV and MVCT systems at 90° to each other, with the potential to utilize the best features of both the systems.

Meeks *et al* (2005) presented a detailed characterization of the Tomotherapy MVCT system. They showed images could be acquired with doses as low as 1.1 cGy (measured in a 20 cm diameter cylindrical phantom). Langen *et al* (2005) presented the use of this system for daily prostate localization, comparing features in MVCT and planning CT scans. Sidhu *et al* (2003) discussed correction of the treatment plan to account for the MVCT dose. Their system used an FPI to acquire 21 conebeam geometry projections at 10° intervals, giving 52.5 cGy in total. The dose level was determined by the requirement of the EPID to receive at least 2.5 cGy per projection. They showed that good dose distributions could be achieved if the MVCT is considered in the plan optimization for IMRT. Pouliot *et al* (2005) used an FPI to achieve conebeam images with 0.02–0.08 monitor units per projection, to produce images with between 5 and 15 cGy. Comparisons between MVCT and treatment CT scans were shown for a head and neck cancer patient. They also showed improvement in image quality by removing the flattening filter from the beam.

4.5. Electromagnetic marker tracking

An approach to the use of surrogate fiducial markers that does not require an x-ray dose is the use of implanted electromagnetic transponders (Balter *et al* 2005, Willoughby *et al* 2006, Kupelian *et al* 2007, Litzenberg *et al* 2007). The transponders used are larger than radio-opaque markers, being cylinders 8 mm long and 1.85 mm diameter (radio-opaque markers are typically 1 mm length e.g. Litzenberg *et al* (2002)) and are imaged, at a rate of 10 Hz, with a magnetic array placed close to the patient surface. Balter *et al* (2005) showed the system to provide submillimetre accuracy under a variety of conditions.

The use of this system has been demonstrated for prostate localization. Willoughby *et al* (2006) presented the first data resulting from imaging sets of three transponders implanted into 20 patients. For 11 of the cases, transponder measurements were compared with kV radiographic imaging of the transponders. The average 3D difference was 1.5 ± 0.9 mm. Patients were also tracked for 8 min and, in some cases, showed organ motion in excess of 1 cm for a large part of this period. Litzenberg *et al* (2007) investigated the potential for

marker migration for all 20 of these patients and showed that 58 of the 60 markers did not migrate, indicating similar long-term stability to radio-opaque markers.

4.6. Ultrasound

As in treatment planning (see section 3.3), ultrasound may be used for soft-tissue visualization to aid the verification process. Often the systems used are based on the same systems as used for treatment planning but are packaged with different software to analyse imaging results in terms of set-up errors and positional corrections needed.

Various ultrasound systems have been developed for soft-tissue verification in radiotherapy, with particular application to prostate localization. The first systems to be implemented consisted of a B-mode trans-abdominal probe attached to a precision tracking arm (Huang *et al* 2002, Chandra *et al* 2003, Little *et al* 2003, Trichter and Ennis 2003, Langen *et al* 2003, Peignaux *et al* 2006). Real-time images were displayed, overlaid with outlines from the planning CT scan. The set-up error was determined by moving the outlines in sagittal and transverse directions until the ultrasound scans matched with them.

Several authors have evaluated the accuracy of such systems in comparison with EPI and have generally found differences. Trichter and Ennis found systematic shifts between the two imaging methods of typically 3 mm in each direction, with a large spread of values. Others have compared ultrasound position measurements with fiducial markers on EPI (Langen *et al* 2003, Van den Heuvel *et al* 2003). Again they show significant systematic differences. Langen reported differences between ultrasound and marker alignment of 0.2 ± 3.7 (1 standard deviation), 2.7 ± 3.9 and 1.6 ± 3.1 mm in anterior–posterior, superior–inferior and lateral directions, respectively. They also found inter-observer variability in the use of the contour alignment system. The significant differences seen in these studies have been attributed to the effects of probe pressure distorting the prostate anatomy. Artignan *et al* (2004) made a systematic study of this effect. Ten volunteers were imaged with a 3D probe fixed with a rigid arm, which was moved stepwise towards the prostate and further images obtained. The largest movement was seen in the posterior direction. A probe displacement of 1.2 cm was needed to get good image quality, resulting in an average prostate displacement of 3.1 mm. McGahan *et al* (2004) made a similar study and found similar results. Treece *et al* (2002) have developed a method of correcting for probe pressure effects. Cury *et al* (2006) compared two approaches to ultrasound verification using a 3D probe system. The first approach (named cross-modality) is equivalent to the techniques described above and the second involves measuring shifts by comparing ultrasound scans on different days. Significant differences were found—6 mm in the superior–inferior direction. They recommended the use of the second approach. Several automatic methods have been developed to outline the prostate in 3D ultrasound scans (Wang *et al* 2003, Hu *et al* 2003).

Although mostly used for prostate radiotherapy, studies of ultrasound localization have been carried out in other sites. Coles *et al* describe localization of the tumour bed in breast radiotherapy using a 3D reconstruction method (Prager *et al* 2002). The post-lumpectomy cavity was visible in all 3D ultrasound images. Comparison with 2D ultrasound showed the 3D system to be significantly superior.

With the advent of fast 3D scanners, several groups are developing real-time tracking systems (Pagoulatos *et al* 2001, Kolen *et al* 2004). Two groups have discussed the use of such as system to gate treatment delivery (Sawada *et al* 2004, Hsu *et al* 2005). The ultimate goal of such approaches would be to gate treatment delivery based on the intra-fraction motion measurement.

4.7. Optical methods

Optical imaging may only provide information on the external anatomy, but may be completely non-invasive and requires zero dose. Its effective use requires knowledge of the relationship between the motion of the target and the external anatomy. Two basic types of system exist: (i) those that use infrared imaging of localized reflective or active markers in order to track motion and (ii) those that use video camera data, which may be used to measure surface outline or to track. One of the first systems developed used a plastic block with infrared markers (Ford *et al* 2002a). Other systems use a set of markers (Soete *et al* 2002, Marmulla *et al* 2004) either attached to the patient's skin or to a holder. These systems are also often used to register the position in the treatment room of the ultrasound systems discussed above. Video systems to track motion have used correlation measurement (Yan *et al* 2002). Video outlining has been achieved using the stereoscopic measurement of the contour of the room laser on the patient surface (Wilks and Bliss 2002), feature-based CT outline matching (Ploeger *et al* 2003) and stereoscopic imaging of a speckle pattern projected onto the patient surface (Moore *et al* 2003, Schöffel *et al* 2007). The intrinsic accuracy of such systems has been shown to be high, with the ability to measure patient shifts of under 1 mm.

Gierga *et al* (2005) evaluated the relationship between internal and external anatomy for liver patients, measured with fluoroscopy of implanted fiducial clips and radio-opaque markers placed on the skin. Results showed the variation in tumour position for a given external marker position ranged between 2 and 9 mm, illustrating the importance of using information on internal anatomy. A solution to this problem is to use external anatomy but to update its relationship with internal anatomy periodically using radiographic images (Kanoulas *et al* 2007).

5. Conclusions

This review has focused on the use of anatomical imaging in radiotherapy, while the accompanying article discusses biological imaging. The combination of information from these complementary imaging modalities is expected to have great synergistic benefit for cancer treatment. This is of particular relevance for target definition, which remains the most important source of error in radiotherapy. Anatomical imaging with CT and MRI yield different gross tumour volumes. Functional imaging with modalities such as PET will generally reveal a different volume still. Thus a decision has to be made how to combine such information. In the absence of good histopathological information, or a proven quantitative biological imaging marker for clonogenic cell density, there is likely to be no gold standard imaging method for a particular treatment case.

Anatomical imaging techniques have an important role to play in image-guided treatment verification. At present several methods are being used as described in the literature. A recent AAPM meeting (Pouliot *et al* 2007) included a debate on the future of IGRT verification, discussing five approaches and finishing with a vote as to which method was going to be the 'winner'. Debates such as this are important, as they encourage discussion of the approaches to IGRT, but it is likely that the optimum solutions will be based on a combination of these approaches as each of the methods have advantages and disadvantages as presented in table 1. Another current area of discussion in IGRT verification is the dose associated with procedures such as kilovoltage conebeam CT. This was also debated at a recent conference (Van Herk and Lomax 2007). Kilovoltage CT is often considered to provide the best imaging information for IGRT, but the dose remains an issue for many, because it potentially involves significant extra skin dose, due to the low x-ray energy used, and delivers a bath of low dose to tissue outside

the target, which may entail the risk of cancer induction. The consequences of this are disease site specific for several reasons. Firstly, the patient age, expected survival and quality of life and disease-recurrence risk vary greatly with disease site and the judgement as to what extra imaging dose is acceptable has to consider these issues. In the case of disease sites where long-term survival is expected to be good, an approach based on a combination of the zero extra dose methods and those that do require extra dose may be the best. A risk-adapted approach to verification is necessary in which a judgement is made as to the trade-off between the risk of the extra dose and the risk of the level of inaccuracy without the use of that technique. This should include consideration of a multimodality approach to verification. A second site-specific consideration is based on radiobiology. There is evidence that several common tumour types exhibit a low α/β ratio (Fowler *et al* 2001, Yarnold *et al* 2005). A consequence of this is that hypofractionation may become a more attractive treatment approach. In this case the dose associated with an x-ray based scan becomes a smaller fraction of the total dose delivered in treatment, hence reducing the relative risk.

The past decade has seen significant advances in medical imaging and in the way imaging is used in radiation therapy. More information than ever may be obtained to assist in designing a patient's treatment, delivering and monitoring the accuracy of that treatment and to following its progress and quantify effectiveness. Debate still exists as to what information is sufficient and how best to harvest that information.

Acknowledgments

The permission granted by authors and journals to reproduce figures in this review is gratefully acknowledged. We had useful discussions with Ellen Donovan, Mike Partridge and Steve Webb during the writing of this review. Rosemary Atkins provided valuable help with the formatting of the references. The work to produce figure 3 was carried out in collaboration with the Radiology Department, Royal Marsden NHS Foundation Trust, Sutton. The work of the radiotherapy physics group is partly funded by Cancer Research UK (under programme reference C46/A3970).

References

Adler J R, Murphy M J, Chang S D and Hancock S L 1999 Image-guided robotic radiosurgery *Neurosurgery* **44** 1299–306

Ahnesjö A 1989 Collapsed cone convolution of radiant energy for photon dose calculation in heterogeneous media *Med. Phys.* **16** 577–92

Ahnesjö A and Aspradakis M M 1999 Dose calculations for external photon beams in radiotherapy *Phys. Med. Biol.* **44** R99–155

Amer A, Marchant T, Sykes J, Czajka J and Moore C 2007 Imaging doses from the Elekta Synergy X-ray cone beam CT system *Br. J. Radiol.* **80** 476–82

Antonuk L E 2002 Electronic portal imaging devices: a review and historical perspective of contemporary technologies and research *Phys. Med. Biol.* **47** R31–R65

Aoki Y, Akanuma A, Evans PM, Lewis D G, Morton E J and Swindell W 1990 A dose distribution evaluation utilizing megavoltage CT imaging, radiation medicine *Med. Imaging Radiat. Oncol.* **8** 107–10

Aoyama H, Shirato H, Nishioka T, Hashimoto S, Tsuchiya K, Kagei K, Onimaru R, Watanabe Y and Miyasaka K 2001 Magnetic resonance imaging system for three-dimensional conformal radiotherapy and its impact on gross tumor volume delineation of central nervous system tumors *Int. J. Radiat. Oncol. Biol. Phys.* **50** 821–7

Artignan X, Smitsmans M H P, Lebesque J V, Jaffray D A, van Her M and Bartelink H 2004 Online ultrasound image guidance for radiotherapy of prostate cancer: impact of image acquisition on prostate displacement *Int. J. Radiat. Oncol. Biol. Phys.* **59** 595–601 1

Aubin S, Beaulieu L, Pouliot S, Pouliot J, Roy R, Girouard L M, Martel-Brisson N, Vigneault E and Laverdiere J 2003 Robustness and precision of an automatic marker detection algorithm for online prostate daily targeting using a standard V-EPID *Med. Phys.* **30** 1825–32

Axel I 1980 Cerebral blood-flow determination by rapid-sequence computed-tomography—a theoretical-analysis *Radiology* **137** 679–86

Bal M and Spies L 2006 Metal artifact reduction in CT using tissue-class modeling and adaptive prefiltering *Med. Phys.* **33** 2852–9

Balter J M, Lam K L, McGinn C J, Lawrence T S and Ten Haken R K 1998 Improvement of CT-based treatment-planning models of abdominal targets using static exhale imaging *Int. J. Radiat. Oncol. Biol. Phys.* **41** 939–43

Balter J M, Ten Haken R K, Lawrence T S, Lam K L and Robertson J M 1996 Uncertainties in CT-based radiation therapy treatment planning associated with patient breathing *Int. J. Radiat. Oncol. Biol. Phys.* **36** 167–74

Balter J M, Wright J N, Newell L J, Friemel B, Dimmer S, Cheng Y, Wong J, Vertatschitsch E and Mate T P 2005 Accuracy of a wireless localization system for radiotherapy *Int. J. Radiat. Oncol. Biol. Phys.* **61** 933–7

Beavis A W, Gibbs P, Dealey R A and Whitton V J 1998 Radiotherapy treatment planning of brain tumours using MRI alone *Br. J. Radiol.* **71** 544–8

Bel A, Vanherk M, Bartelink H and Lebesque J V 1993 A verification procedure to improve patient set-up accuracy using portal images *Radiother. Oncol.* **29** 253–60

Berbeco R I, Jiang S B, Sharp G C, Chen G T Y, Mostafavi H and Shirato H 2004 Integrated radiotherapy imaging system (IRIS): design considerations of tumour tracking with linac gantry-mounted diagnostic x-ray systems with flat-panel detectors *Phys. Med. Biol.* **49** 243–55

Biggs P J, Goitein M and Russell M D 1985 A diagnostic X-ray field verification device for a 10 MV linear-accelerator *Int. J. Radiat. Oncol. Biol. Phys.* **11** 635–43

Blasko J C, Grimm P D and Ragde H 1993 Brachytherapy and organ preservation in the management of carcinoma of the prostate *Semin. Radiat. Oncol.* **3** 240–9

Blasko J C, Wallner K, Grimm P D and Ragde H 1995 Prostate-specific antigen based disease-control following ultrasound-guided (125) iodine implantation for stage T1/T2 prostatic-carcinoma *J. Urol.* **154** 1096–9

Bortfeld T, Jokivarsi K, Goitein M, Kung J and Jiang S B 2002 Effects of intra-fraction motion on IMRT dose delivery: statistical analysis and simulation *Phys. Med. Biol.* **47** 2203–20

Boyer A L, Antonuk L, Fenster A, Vanherk M, Meertens H, Munro P, Reinstein L E and Wong J 1992 A review of electronic portal imaging devices (EPIDs) *Med. Phys.* **19** 1–16

Brahme A 1988 Optimization of stationary and moving beam radiation-therapy techniques *Radiother. Oncol.* **12** 129–40

Brahme A, Lind B and Nafstadius P 1987 Radiotherapeutic computed-tomography with scanned photon beams *Int. J. Radiat. Oncol. Biol. Phys.* **13** 95–101

Burnside E S, Hall T J, Sommer A M, Hesley G K, Sisney G A, Svensson W E, Fine J P, Jiang J J and Hangiandreou N J 2007 Differentiating benign from malignant solid breast masses with US strain imaging *Radiology* **245** 401–10

Cassell K J, Hobday P A and Parker R P 1981 The implementation of a generalized batho inhomogeneity correction for radiotherapy planning with direct use of CT numbers *Phys. Med. Biol.* **26** 825–33

Castellano I A 2006 Optimisation of radiation dose to patients in computed tomography *PhD thesis* University of London, London, UK

Cha S, Knopp E A, Johnson G, Wetzel S G, Litt A W and Zagzag D 2002 Intracranial mass lesions: dynamic contrast-enhanced susceptibility-weighted echo-planar perfusion MR imaging *Radiology* **223** 11–29

Chandra A, Dong L, Huang E, Kuban D A, O'Neill L, Rosen I and Pollack A 2003 Experience of ultrasound-based daily prostate localization *Int. J. Radiat. Oncol. Biol. Phys.* **56** 436–47

Chang C C, Chen M K, Wu H K and Liu M T 2002 Nasopharyngeal carcinoma volume measurements determined with computed tomography: study of intraobserver and interobserver variability *J. Otolaryngol.* **31** 361–5

Chao K S C, Bosch W R, Mutic S, Lewis J S, Dehdashti F, Mintun M A, Dempsey J F, Perez C A, Purdy J A and Welch M J 2001 A novel approach to overcome hypoxic tumor resistance: Cu-ATSM-guided intensity-modulated radiation therapy *Int. J. Radiat. Oncol. Biol. Phys.* **49** 1171–82

Chen G T Y, Singh R P, Castro Jr, Lyman J T and Quivey J M 1979 Treatment planning for heavy-ion radiotherapy *Int. J. Radiat. Oncol. Biol. Phys.* **5** 1809–19

Chen J, Lee R J, Handrahan D and Sause W T 2007 Intensity-modulated radiotherapy using implanted fiducial markers with daily portal imaging: assessment of prostate organ motion *Int. J. Radiat. Oncol. Biol. Phys.* **68** 912–9

Chen Q S, Weinhous M S, Deibel F C, Ciezki J P and Macklis R M 2001 Fluoroscopic study of tumor motion due to breathing: facilitating precise radiation therapy for lung cancer patients *Med. Phys.* **28** 1850–6

Chenevert T L, Stegman L D, Taylor J M G, Robertson P L, Greenberg H S, Rehemtulla A and Ross B D 2000 Diffusion magnetic resonance imaging: an early surrogate marker of therapeutic efficacy in brain tumors *J. Natl. Cancer Inst.* **92** 2029–36

Cheung P C F, Sixel K E, Tirona R and Ung Y C 2003 Reproducibility of lung tumor position and reduction of lung mass within the planning target volume using active breathing control (ABC) *Int. J. Radiat. Oncol. Biol. Phys.* **57** 1437–42

Choi Y M, Kim J K, Lee H S, Hur W J, Hong Y S, Park S, Ahn K and Cho H L 2006 Influence of intravenous contrast agent on dose calculations of intensity modulated radiation therapy plans for head and neck cancer *Radiother. Oncol.* **81** 158–62

Christensen G E *et al* 2001 Image-based dose planning of intracavitary brachytherapy: registration of serial-imaging studies using deformable anatomic templates *Int. J. Radiat. Oncol. Biol. Phys.* **51** 227–43

Coles C E *et al* 2007 High definition three-dimensional ultrasound to localise the tumour bed: a breast radiotherapy planning study *Radiother. Oncol.* **84** 233–41

Coolens C and Childs P J 2003 Calibration of CT Hounsfield units for radiotherapy treatment planning of patients with metallic hip prostheses: the use of the extended CT-scale *Phys. Med. Biol.* **48** 1591–603

Coolens C, Evans P M, Seco J, Webb S, Blackall J M, Rietzel E and Chen G T Y 2006 The susceptibility of IMRT dose distributions to intrafraction organ motion: an investigation into smoothing filters derived from four dimensional computed tomography data *Med. Phys.* **33** 2809–18

Court L, Rosen I, Mohan R and Dong L 2003 Evaluation of mechanical precision and alignment uncertainties for an integrated CT/LINAC system *Med. Phys.* **30** 1198–210

Creutzberg C L, Althof V G M, Huizenga H, Visser A G and Levendag P C 1993 Quality assurance using portal imaging—the accuracy of patient positioning in irradiation of breast-cancer *Int. J. Radiat. Oncol. Biol. Phys.* **25** 529–39

Crook J M, Raymond Y, Salhani D, Yang H and Esche B 1995 Prostate motion during standard radiotherapy as assessed by fiducial markers *Radiother. Oncol.* **37** 35–42

Cury F L B, Shenouda G, Souhami L, Duclos M, Faria S L, David M, Verhaegen F, Corns R and Falco T 2006 Ultrasound-based image guided radiotherapy for prostate cancer—comparison of cross-modality and intramodality methods for daily localization during external beam radiotherapy *Int. J. Radiat. Oncol. Biol. Phys.* **66** 1562–7

Dawson L A, Brock K K, Kazanjian S, Fitch D, McGinn C J, Lawrence T S, Ten Haken R K and Balter J 2001 The reproducibility of organ position using active breathing control (ABC) during liver radiotherapy *Int. J. Radiat. Oncol. Biol. Phys.* **51** 1410–21

De Boer H C J and Heijmen B J M 2001 A protocol for the reduction of systematic patient setup errors with minimal portal imaging workload *Int. J. Radiat. Oncol. Biol. Phys.* **50** 1350–65

De Boer H C J and Heijmen B J M 2007 eNAL: an extension of the NAL setup correction protocol for effective use of weekly follow-up measurements *Int. J. Radiat. Oncol. Biol. Phys.* **67** 1586–95

De Boer J C J, Heijmen B J M, Pasma K L and Visser A G 2000 Characterization of a high-elbow, fluoroscopic electronic portal imaging device for portal dosimetry *Phys. Med. Biol.* **45** 197–216

DeBiose D A, Horwitz E M, Martinez A A, Edmundson G K, Chen P Y, Gustafson G S, Madrazo B, Wimbish K, Mele E and Vicini F A 1997 The use of ultrasonography in the localization of the lumpectomy cavity for interstitial brachytherapy of the breast *Int. J. Radiat. Oncol. Biol. Phys.* **38** 755–9

Debois M *et al* 1999 The contribution of magnetic resonance imaging to the three-dimensional treatment planning of localized prostate cancer *Int. J. Radiat. Oncol. Biol. Phys.* **45** 857–65

De la Zerda A, Armbruster B and Xing L 2007 Formulating adaptive radiation therapy (ART) treatment planning into a closed-loop control framework *Phys. Med. Biol.* **52** 4137–53

De Neve W, Vandenheuvel F, Debeukeleer M, Coghe M, Thon L, Deroover P, Vanlancker M and Storme G 1992 Routine clinical online portal imaging followed by immediate field adjustment using a tele-controlled patient couch *Radiother. Oncol.* **24** 45–54

Ding G X, Duggan D M and Coffey C W 2007 Characteristics of kilovoltage x-ray beams used for cone-beam computed tomography in radiation therapy *Phys. Med. Biol.* **52** 1595–615

Elgayed Aah, Bel A, Vijlbrief R, Bartelink H and Lebesque Jv 1993 Time trend of patient setup deviations during pelvic irradiation using electronic portal imaging *Radiother. Oncol* **26** 162–71

Endo M, Tsunoo T, Nakamori N and Yoshida K 2001 Effect of scattered radiation on image noise in cone beam CT *Med. Phys.* **28** 469–74

Evans P M, Coolens C and Nioutsikou E 2006a Effects of averaging over motion and the resulting systematic errors in radiation therapy *Phys. Med. Biol.* **51** N1–7

Evans P M, Mosleh-Shirazi M A, Harris E J and Seco J 2006b Monte Carlo and Lambertian light guide models of the light output from scintillation crystals at megavoltage energies *Med. Phys.* **33** 1797–809

Ezz A, Munro P, Porter A T, Battista J, Jaffray Da, Fenster A and Osborne S 1992 Daily monitoring and correction of radiation-field placement using a video-based portal imaging-system—a pilot-study *Int. J. Radiat. Oncol. Biol. Phys.* **22** 159–65

Featherstone C, Harnett A N and Brunt A M 1999 Ultrasound localization of the ovaries for radiation-induced ovarian ablation *Clin. Oncol.* **11** 393–7

Feldkamp L A, Davis L C and Kress J W 1984 Practical cone-beam algorithm *J. Opt. Soc. Am.* A **1** 612–9

Fiorino C, Reni M, Bolognesi A, Cattaneo G M and Calandrino R 1998 Intra- and inter-observer variability in contouring prostate and seminal vesicles: implications for conformal treatment planning *Radiother. Oncol.* **47** 285–92

Ford E C, Chang J, Mueller K, Sidhu K, Todor D, Mageras G, Yorke E, Ling C C and Amols H 2002b Cone-beam CT with megavoltage beams and an amorphous silicon electronic portal imaging device: potential for verification of radiotherapy of lung cancer *Med. Phys.* **29** 2913–24

Ford E C, Mageras G S, Yorke E, Rosenzweig K E, Wagman R and Ling C C 2002a Evaluation of respiratory movement during gated radiotherapy using film and electronic portal imaging *Int. J. Radiat. Oncol. Biol. Phys.* **52** 522–31

Forrest L J, Mackie T R, Ruchala K, Turek M, Kapatoes J, Jaradat H, Hui S, Balog J, Vail D M and Mehta M P 2004 The utility of megavoltage computed tomography images from a helical tomotherapy system for set-up verification purposes *Int. J. Radiat. Oncol. Biol. Phys.* **60** 1639–44

Fowler J, Rick Chappell R and Ritter M 2001 Is α/β for prostate tumors really low? *Int. J. Radiat. Oncol. Biol. Phys.* **50** 1021–31

Fransson P, Bergstrom P, Lofroth P O and Widmark A 2002 Prospective evaluation of urinary and intestinal side effects after BeamCath® stereotactic dose-escalated radiotherapy of prostate cancer *Radiother. Oncol.* **63** 239–48

Gierga D P, Brewer J, Sharp G C, Betke M, Willett C G and Chen G T Y 2005 The correlation between internal and external markers for abdominal tumors: implications for respiratory gating *Int. J. Radiat. Oncol. Biol. Phys.* **61** 1551–8

Gildersleve J, Dearnaley D P, Evans P M, Law M, Rawlings C and Swindell W 1994 A randomized trial of patient repositioning during radiotherapy using a megavoltage imaging-system *Radiother. Oncol.* **31** 161–8

Gill S S, Thomas D G T, Warrington A P and Brada M 1991 Relocatable frame for stereotaxic external beam radiotherapy *Int. J. Radiat. Oncol. Biol. Phys.* **20** 599–603

Greer P B 2005 Correction of pixel sensitivity variation and off-axis response for amorphous silicon EPID dosimetry *Med. Phys.* **32** 3558–68

Grosu A L, Piert M, Weber W A, Jeremic B, Picchio M, Schratzenstaller U, Zimmermann F B, Schwaiger M and Molls M 2005 Positron emission tomography for radiation treatment planning *Strahlenther. Onkol.* **181** 483–99

Gustafsson A, Lind B K and Brahme A 1994 A generalized pencil beam algorithm for optimization of radiation-therapy *Med. Phys.* **21** 343–57

Hakime A, Peddi H, Hines-Peralta A U, Wilcox C J, Kruskal J, Lin S Z, de Baere T, Raptopoulos V D and Goldberg S N 2007 CT perfusion for determination of pharmacologically mediated blood flow changes in an animal tumor model *Radiology* **243** 712–9

Hamilton C S and Ebert M A 2005 Volumetric uncertainty in radiotherapy *Clin. Oncol.* **17** 456–64

Hanley J *et al* 1999 Deep inspiration breath-hold technique for lung tumors: the potential value of target immobilization and reduced lung density in dose escalation *Int. J. Radiat. Oncol. Biol. Phys.* **45** 603–11

Hansen V N, Evans P M and Swindell W 1996 The application of transit dosimetry to precision radiotherapy *Med. Phys.* **23** 713–21

Hartkens T, Rohr K and Stiehl H S 2002 Evaluation of 3D operators for the detection of anatomical point landmarks in MR and CT images *Comput. Vis. Image Underst.* **86** 118–36

Hector C L, Webb S and Evans P M 2000 The dosimetric consequences of inter-fractional patient movement on conventional and intensity-modulated breast radiotherapy treatments *Radiother. Oncol.* **54** 57–64

Helyer S J, Moskovic E, Ashley S, Hastings L and Yarnold J R 1999 A study testing the routine use of ultrasound measurements when selecting the electron energy for breast boost radiotherapy *Clin. Oncol.* **11** 164–8

Henry A M *et al* 2006 X-ray volume imaging in bladder radiotherapy verification *Int. J. Radiat. Oncol. Biol. Phys.* **64** 1174–8

Henson P W and Fox R A 1984 The electron-density of bone for inhomogeneity correction in radiotherapy planning using CT numbers *Phys. Med. Biol.* **29** 351–9

Herman M G 2005 Clinical use of electronic portal imaging *Semin. Radiat. Oncol.* **15** 157–67

Herman M G, Balter J M, Jaffray D A, McGee K P, Munro P, Shalev S, Van Herk M and Wong J W 2001 Clinical use of electronic portal imaging: Report of AAPM radiation therapy committee Task Group 58 *Med. Phys.* **28** 712–37

Hermans R, Lambin P, Van der Goten A, Van den Bogaert W, Verbist B, Weltens C and Delaere P R 1999 Tumoural perfusion as measured by dynamic computed tomography in head and neck carcinoma *Radiother. Oncol.* **53** 105–11

Hermans R, Meijerink M, Van den Bogaert W, Rijnders A, Weltens C and Lambin P 2003 Tumor perfusion rate determined noninvasively by dynamic computed tomography predicts outcome in head-and-neck cancer after radiotherapy *Int. J. Radiat. Oncol. Biol. Phys.* **57** 1351–6

Hesse B M, Spies L and Groh B A 1998 Tomotherapeutic portal imaging for radiation treatment verification *Phys. Med. Biol.* **43** 3607–16

Hill D L G, Batchelor P G, Holden M and Hawkes D J 2001 Medical image registration *Phys. Med. Biol.* **46** R1–45

Hoskin P J and Bownes P 2006 Innovative technologies in radiation therapy: brachytherapy *Semin. Radiat. Oncol.* **16** 209–17

Hounsfield G N 1973 Computerized transverse axial scanning (tomography): 1. Description of system *Br. J. Radiol.* **46** 1016–22

Hsu A, Miller N R, Evans P M, Bamber J C and Webb S 2005 Feasibility of using ultrasound for real-time tracking during radiotherapy *Med. Phys.* **32** 1500–12

Hu N, Downey D B, Fenster A and Ladak H M 2003 Prostate boundary segmentation from 3D ultrasound images *Med. Phys.* **30** 1648–59

Huang E, Dong L, Chandra A, Kuban D A, Rosen I I, Evans A and Pollack A 2002 Intrafraction prostate motion during IMRT for prostate cancer *Int. J. Radiat. Oncol. Biol. Phys.* **53** 261–8

Hurkmans C W, Remeijer P, Lebesque J V and Mijnheer B J 2001 Set-up verification using portal imaging; review of current clinical practice *Radiother. Oncol.* **58** 105–20

International Commission on Radiation Units and Measurement 1993 Prescribing, Recording and Reporting Photon Beam Therapy *ICRU Report 50* (Bethesda, MD: ICRU)

International Commission on Radiation Units and Measurement 1999 Prescribing, Recording and Reporting Photon Beam Therapy (supplement to ICRU Report 50) *ICRU Report 62* (Bethesda, MD: ICRU)

Islam M K, Purdie T G, Norrlinger B D, Alasti H, Moseley D J, Sharpe M B, Siewerdsen J H and Jaffray D A 2006 Patient dose from kilovoltage cone beam computed tomography imaging in radiation therapy *Med. Phys.* **33** 1573–82

Jackson A S N, Reinsberg S A, Sohaib S A, Charles-Edwards E M, Mangar S A, South C P, Leach M O and Dearnaley D P 2007 Distortion-corrected T2 weighted MRI: a novel approach to prostate radiotherapy planning *Br. J. Radiol.* **80** 926–33

Jaffray D A 2005 Emergent technologies for 3-dimensional image-guided radiation delivery *Semin. Radiat. Oncol.* **15** 208–16

Jaffray D A 2007 Image-guided radiation therapy: from concept to practice *Semin. Radiat. Oncol.* **17** 243–4

Jaffray D A, Chawla K, Yu C and Wong J W 1995 Dual-beam imaging for online verification of radiotherapy field placement *Int. J. Radiat. Oncol. Biol. Phys.* **33** 1273–80

Jaffray D A, Drake D G, Moreau M, Martinez A A and Wong J W 1999 A radiographic and tomographic imaging system integrated into a medical linear accelerator for localization of bone and soft-tissue targets *Int. J. Radiat. Oncol. Biol. Phys.* **45** 773–89

Jaffray D A and Siewerdsen J H 2000 Cone-beam computed tomography with a flat-panel imager: initial performance characterization *Med. Phys.* **27** 1311–23

Jaffray D A, Siewerdsen J H, Wong J W and Martinez A A 2002 Flat-panel cone-beam computed tomography for image-guided radiation therapy *Int. J. Radiat. Oncol. Biol. Phys.* **53** 1337–49

Jäkel O, Jacob C, Schardt D, Karger C P and Hartmann D H 2001a Relation between carbon ion ranges and x-ray CT numbers *Med. Phys.* **28** 701–3

Jäkel O, Krämer M, Karger C P and Debus J 2001b Treatment planning for heavy ion radiotherapy: clinical implementation and application *Phys. Med. Biol.* **46** 1101–16

Jäkel O and Reiss P 2007 The influence of metal artefacts on the range of ion beams *Phys. Med. Biol.* **52** 635–44

Jarry G, Graham S A, Moseley D J, Jaffray D J, Siewerdsen J H and Verhaegen F 2006 Characterization of scattered radiation in kV CBCT images using Monte Carlo simulations *Med. Phys.* **33** 4320–9

Jiang S B 2006 Radiotherapy of mobile tumors *Semin. Radiat. Oncol.* **16** 239–48

Jin J Y, Ajlouni M, Ryu S, Chen Q, Li S D and Movsas B 2007 A technique of quantitatively monitoring both respiratory and nonrespiratory motion in patients using external body markers *Med. Phys.* **34** 2875–81

Kalender W A 2006 X-ray computed tomography *Phys. Med. Biol.* **51** R29–43

Kalender W A, Seissler W and Vock P 1989 Single-breath-hold spiral volumetric CT by continuous patient translation and scanning rotation *Radiology* **173** 414

Kanoulas E, Aslam J A, Sharp G C, Berbeco R I, Nishioka S, Shirato H and Jiang S B 2007 Derivation of the tumor position from external respiratory surrogates with periodical updating of the internal/external correlation *Phys. Med. Biol.* **52** 5443–56

Kapatoes J M, Olivera G H, Balog J P, Keller H, Reckwerdt P J and Mackie T R 2001 On the accuracy and effectiveness of dose reconstruction for tomotherapy *Phys. Med. Biol.* **46** 943–66

Keall P 2004 4-dimensional computed tomography imaging and treatment planning *Semin. Radiat. Oncol.* **14** 81–90

Keall P J, Starkschall G, Shukla H, Forster K M, Ortiz V, Stevens C W, Vedam S S, George R, Guerrero T and Mohan R 2004 Acquiring 4D thoracic CT scans using a multislice helical method *Phys. Med. Biol.* **49** 2053–67

Keston P, Murray A D and Jackson A 2003 Cerebral perfusion imaging using contrast-enhanced MRI *Clin. Radiol.* **58** 505–13

Khoo V S, Adams E J, Saran F, Bedford J L, Perks J R, Warrington A P and Brada M 2000 A comparison of clinical target volumes determined by CT and MRI for the radiotherapy planning of base of skull meningiomas *Int. J. Radiat. Oncol. Biol. Phys.* **46** 1309–17

Khoo V S and Joon D L 2006 New developments in mill for target volume delineation in radiotherapy *Br. J. Radiol.* **79** S2–15

Kijewski P K and Bjarngard B E 1978 Use of computed tomography data for radiotherapy dose calculations *Int. J. Radiat. Oncol. Biol. Phys.* **4** 429–35

Kirby M C and Glendinning A G 2006 Developments in electronic portal imaging systems *Br. J. Radiol.* **79** S50–S65

Kolen A F, Miller N R, Ahmed E E and Bamber J C 2004 Characterization of cardiovascular liver motion for the eventual application of elasticity imaging to the liver in vivo *Phys. Med. Biol.* **49** 4187–206

Kooy H M, Vanherk M, Barnes P D, Alexander E, Dunbar S F, Tarbell N J, Mulkern R V, Holupka E J and Loeffler J S 1994 Image fusion for stereotaxic radiotherapy and radiosurgery treatment planning *Int. J. Radiat. Oncol. Biol. Phys.* **28** 1229–34

Kubo H D and Hill B C 1996 Respiration gated radiotherapy treatment: a technical study *Phys. Med. Biol.* **41** 83–91

Kupelian P *et al* 2007 Multi-institutional clinical experience with the Calypso System in localization and continuous, real-time monitoring of the prostate gland during external radiotherapy *Int. J. Radiat. Oncol. Biol. Phys.* **67** 1088–98

Kuriyama K, Onishi H, Sano N, Komiyama T, Aikawa Y, Tateda Y, Araki T and Uematsu M 2003 A new irradiation unit constructed of self-moving gantry-CT and linac *Int. J. Radiat. Oncol. Biol. Phys.* **55** 428–35

Lagerwaard F J, de Koste J R V, Nijssen-Visser M R J, Schuchhard-Schipper R H, Oei S S, Munne A and Senan S 2001 Multiple "slow" CT scans for incorporating lung tumor mobility in radiotherapy planning *Int. J. Radiat. Oncol. Biol. Phys.* **51** 932–7

Land I, Mills J A, Young K, Haas O, Wilson A and Burnham K J 2007 Modelling target coverage for respiratory-gated radiotherapy with simulated and real breathing traces *Strahlenther. Onkol.* **183** 19–20

Langen K M *et al* 2003 Evaluation of ultrasound-based prostate localization for image-guided radiotherapy *Int. J. Radiat. Oncol. Biol. Phys.* **57** 635–44

Langen K M, Meeks S L, Poole D O, Wagner T H, Willoughby T R, Kupelian P A, Ruchala K J, Haimerl J and Olivera G H 2005 The use of megavoltage CT (MVCT) images for dose recomputations *Phys. Med. Biol.* **50** 4259–76

Langmack K A 2001 Portal imaging *Br. J. Radiol.* **74** 789–804

Lawton C A, DeSilvio M, Lee W R, Gomella L, Grignon D, Gillin M, Morton G, Pisansky T and Sandler H 2007 Results of a phase II trial of transrectal ultrasound-guided permanent radioactive implantation of the prostate for definitive management of localized adenocarcinoma of the prostate (Radiation Therapy Oncology Group 98–05) *Int. J. Radiat. Oncol. Biol. Phys.* **67** 39–47

Lee Y K, Bollet M, Charles-Edwards G, Flower M A, Leach M O, McNair H, Moore E, Rowbottom C and Webb S 2003 Radiotherapy treatment planning of prostate cancer using magnetic resonance imaging alone *Radiother. Oncol.* **66** 203–16

Létourneau D, Wong R, Moseley D, Sharpe M B, Ansell S, Gospodarowicz M and Jaffray D A 2007 Online planning and delivery technique for radiotherapy of spinal metastases using cone-beam CT: image quality and system performance *Int. J. Radiation Oncology Biol. Phys.* **67** 1229–37

Létourneau D, Wong J W, Oldham M, Gulam M, Watt L, Jaffray D A, Siewerdsen J H and Martinez A A 2005 Cone-beam-CT guided radiation therapy: technical implementation *Radiother. Oncol.* **75** 279–86

Lewis D G, Swindell W, Morton E J, Evans P M and Xiao Z R 1992 A megavoltage CT Scanner for radiotherapy verification *Phys. Med. Biol.* **37** 1985–99

Lewis M A 2001 Multislice CT: opportunities and challenges *Br. J. Radiol.* **74** 779–81

Little D J, Dong L, Levy L B, Chandra A and Kuban D A 2003 Use of portal images and bat ultrasonography to measure setup error and organ motion for prostate IMRT: Implications for treatment margins *Int. J. Radiat. Oncol. Biol. Phys.* **56** 1218–24

Litzenberg D, Dawson L A, Sandler H, Sanda M G, McShan D L, Ten Haken R K, Lam K L, Brock K K and Balter J M 2002 Daily prostate targeting using implanted radio-opaque markers *Int. J. Rad. Oncol. Biol. Phys.* **52** 699–703

Litzenberg D W *et al* 2007 Positional stability of electro-magnetic transponders used for prostate localization and continuous, real-time tracking *Int. J. Radiat. Oncol. Biol. Phys.* **68** 1199–206

Low D A, Nystrom M, Kalinin E, Parikh P, Dempsey J F, Bradley J D, Mutic S, Wahab S H, Islam T, Christensen G, Politte D G and Whiting B R 2003 A method for the reconstruction of four-dimensional synchronized CT scans acquired during free breathing *Med. Phys.* **30** 1254–63

Low D, Parikh P, Lu W, Dempsey J, Wahab S, Hubenschmidt J, Nystrom M, Handoko M and Bradley J 2005 Novel breathing motion model for radiotherapy *Int. J. Rad. Oncol. Biol. Phys.* **63** 921–9

Lu H M, Cash E, Chen M H, Chin L, Manning W J, Harris J and Bornstein B 2000 Reduction of cardiac volume in left-breast treatment fields by respiratory maneuvers: a CT study *Int. J. Radiat. Oncol. Biol. Phys.* **47** 895–904

Lu W G, Olivera G H, Chen Q, Ruchala K J, Haimerl J, Meeks S L, Langen K M and Kupelian P A 2006a Deformable registration of the planning image (kVCT) and the daily images (MVCT) for adaptive radiation therapy *Phys. Med. Biol.* **51** 4357–74

Lu W G, Parikh P J, Hubenschmidt J P, Bradley J D and Low D A 2006b A comparison between amplitude sorting and phase-angle sorting using external respiratory measurement for 4D CT *Med. Phys.* **33** 2964–74

Lujan A E, Larsen E W, Balter J M and Ten Haken R K 1999 A method for incorporating organ motion due to breathing into 3D dose calculations *Med. Phys.* **26** 715–20

Ma C M and Paskalev K 2006 In-room CT techniques for image-guided radiation therapy *Med. Dosim.* **31** 30–9

Machtay M, Lanciano R, Hoffman J and Hanks G E 1994 Inaccuracies in using the lumpectomy scar for planning electron boosts in primary breast-carcinoma *Int. J. Radiat. Oncol. Biol. Phys.* **30** 43–8

Mackie T R, Balog J, Ruchala K, Shepard D, Aldridge S, Fitchard E, Reckwerdt P, Olivera G, McNutt T and Mehta M 1999 Tomotherapy *Semin. Radiat. Oncol.* **9** 108–17

Mageras G S and Yorke E 2004 Deep inspiration breath hold and respiratory gating strategies for reducing organ motion in radiation treatment *Semin. Radiat. Oncol.* **14** 65–75

Malone S, Crook J M, Kendal W S and Szanto J 2000 Respiratory-induced prostate motion: quantification and characterization *Int. J. Radiat. Oncol. Biol. Phys.* **48** 105–9

Malušek A, Seger M M, Sandborg M and Carlsson G A 2005 Effect of scatter on reconstructed image quality in cone beam computed tomography: evaluation of a scatter-reduction optimisation function *Radiat. Prot. Dosim.* **114** 337–40

Mansfield P 2004 Snapshot magnetic resonance imaging (Nobel lecture) *Angewandte Chemie-International* **43** 5456–64

Marks L B, Hebert M E, Bentel G, Spencer D P, Sherouse G W and Prosnitz L R 1994 To treat or not to treat the internal mammary nodes—a possible compromise *Int. J. Radiat. Oncol. Biol. Phys.* **29** 903–9

Marmulla R, Luth T, Muhling J and Hassfeld S 2004 Markerless laser registration in image-guided oral and maxillofacial surgery *J. Oral Maxillofac. Surg.* **62** 845–51

Martinez A A, Yan D, Lockman D, Brabbins D, Kota K, Sharpe M, Jaffray D A, Vicini F and Wong J 2001 Improvement in dose escalation using the process of adaptive radiotherapy combined with three-dimensional conformal or intensity-modulated beams for prostate cancer *Int. J. Radiat. Oncol. Biol. Phys.* **50** 1226–34

McClelland J R, Webb S, McQuaid D, Binnie D M and Hawkes D J 2007 Tracking 'differential organ motion' with a 'breathing' multileaf collimator: magnitude of problem assessed using 4D CT data and a motion-compensation strategy *Phys. Med. Biol.* **52** 4805–26

McCurdy B M C, Luchka K and Pistorius S 2001 Dosimetric investigation and portal dose image prediction using an amorphous silicon electronic portal imaging device *Med. Phys.* **28** 911–24

McDermott L N, Louwe R J W, Sonke J J, van Herk M B and Mijnheer B J 2004 Dose-response and ghosting effects of an amorphous silicon electronic portal imaging device *Med. Phys.* **31** 285–95

McDermott L N, Wendling M, Sonke J J, van Herk M and Mijnheer B J 2006 Anatomy changes in radiotherapy detected using portal imaging *Radiother. Oncol.* **79** 211–7

McGahan J P, Ryu J and Fogata M 2004 Ultrasound probe pressure as a source of error in prostate localization for external beam radiotherapy *Int. J. Radiat. Oncol. Biol. Phys.* **60** 788–93

McKenzie A L, van Herk M and Mijnheer B 2000 The width of margins in radiotherapy treatment plans *Phys. Med. Biol.* **45** 3331–42

McKenzie A L, van Herk M and Mijnheer B 2002 Margins for geometric uncertainty around organs at risk in radiotherapy *Radiother. Oncol.* **62** 299–307

McNutt T R, Mackie T R, Reckwerdt P and Paliwal B R 1996 Modeling dose distributions from portal dose images using the convolution/superposition method *Med. Phys.* **23** 1381–92

McQuaid D and Webb S 2006 IMRT delivery to a moving target by dynamic MLC tracking: delivery for targets moving in two dimensions in the beam's eye view *Phys. Med. Biol.* **51** 4819–39

Meeks S L, Harmon J F, Langen K M, Willoughby T R, Wagner T H and Kupelian P A 2005 Performance characterization of megavoltage computed tomography imaging on a helical tomotherapy unit *Med. Phys.* **32** 2673–81

Merrick G S, Butler W M, Dorsey A T, Lief J H, Walbert H L and Blatt H J 1999 Rectal dosimetric analysis following prostate brachytherapy *Int. J. Radiat. Oncol. Biol. Phys.* **43** 1021–7

Milan J and Bentley R E 1974 Storage an manipulation of radiation-dose data in a small digital computer *Br. J. Radiol.* **47** 115–21

Miles K A and Griffiths M R 2003 Perfusion CT: a worthwhile enhancement? *Br. J. Radiol.* **76** 220–31

Minohara S, Kanai T, Endo M, Noda K and Kanazawa M 2000 Respiratory gated irradiation system for heavy-ion radiotherapy *Int. J. Radiat. Oncol. Biol. Phys.* **47** 1097–103

Moore C, Lilley F, Sauret V, Lalor M and Burton D 2003 Opto-electronic sensing of body surface topology changes during radiotherapy for rectal cancer *Int. J. Radiat. Oncol. Biol. Phys.* **56** 248–58

Morin O, Chen J, Aubin M, Gillis A, Aubry J F, Bose S, Chen H, Descovich M, Xia P and Pouliot J 2007 Dose calculation using megavoltage cone-beam CT *Int. J. Radiat. Oncol. Biol. Phys.* **67** 1201–10

Mosleh-Shirazi M A, Evans P M, Swindell W, Symonds-Tayler J R N, Webb S and Partridge M 1998a Rapid portal imaging with a high-efficiency, large field-of-view detector *Med. Phys.* **25** 2333–46

Mosleh-Shirazi M A, Evans P M, Swindell W, Webb S and Partridge M 1998b A cone-beam megavoltage CT scanner for treatment verification in conformal radiotherapy *Radiother. Oncol.* **48** 319–28

Mukherji S K *et al* 2005 Interobserver reliability of computed tomography derived primary tumor volume measurement in patients with supraglottic carcinoma *Cancer* **103** 2616–22

Murphy M J, Chang S D, Gibbs I C, Le Q T, Hai J, Kim D, Martin D P and Adler J R 2003 Patterns of patient movement during frameless image-guided radiosurgery *Int. J. Radiat. Oncol. Biol. Phys.* **55** 1400–8

Mustafa A A and Jackson D F 1983 The relation between x-ray ct numbers and charged-particle stopping powers and its significance for radiotherapy treatment planning *Phys. Med. Biol.* **28** 169–76

Nabavi D G, Cenic A, Craen R A, Gelb A W, Bennett J D, Kozak R and Lee T Y 1999 CT assessment of cerebral perfusion: experimental validation and initial clinical experience *Radiology* **213** 141–9

Nagakawa K, Aoki Y, Akanuma A, Onogi Y, Karasawa K, Terahara A, Hasezawa K and Sasaki Y 1991 Development of a megavoltage CT scanner using linear accelerator treatment beam *J. Japan. Soc. Ther. Radiol. Oncol.* **3** 265–76

Nalder C A, Bidmead A M, Mubata C D, Tait D and Beardmore C 2001 Influence of a vac-fix immobilization device on the accuracy of patient positioning during routine breast radiotherapy *Br. J. Radiol.* **74** 249–54

Nederveen A J, Dehnad H, van der Heide U A, van Moorselaar R J A, Hofman P and Lagendijk J J W 2003 Comparison of megavoltage position verification for prostate irradiation based on bony anatomy and implanted fiducials *Radiother. Oncol.* **68** 81–8

Nederveen A J, van der Heide U A, Dehnad H, van Moorselaar R J A, Hofman P and Lagendijk J J W 2002 Measurements and clinical consequences of prostate motion during a radiotherapy fraction *Int. J. Radiat. Oncol. Biol. Phys.* **53** 206–14

Nestle U, Weber W and Grosu A L 2008 Biological imaging in radiation therapy: role of PET *Phys. Med. Biol.* (in press)

Newbold K, Sohaib A, Castellano I, Mears D, A'Hern R, Rhys-Evans P, Fisher C, Harrington K and Nutting C 2005 Validation of perfusion computed tomography (CT) parameters as surrogate markers of hypoxia in squamous cell carcinoma of the head and neck *EJC Suppl.* **3** 400

Nishidai T, Nagata Y, Takahashi M, Abe M, Yamaoka N, Ishihara H, Kubo Y, Ohta H and Kazusa C 1990 CT simulator—a new 3-D planning and simulating system for radiotherapy: 1. Description of system *Int. J. Radiat. Oncol. Biol. Phys.* **18** 499–504

O'Connor J E 1957 The variation of scattered X-rays with density in an irradiated body *Phys. Med. Biol.* **1** 352–69

Ohara K, Okumura T, Akisada M, Inada T, Mori T, Yokota H and Calaguas M J B 1989 Irradiation synchronized with respiration gate *Int. J. Radiat. Oncol. Biol. Phys.* **17** 853–7

Ohnesorge B, Flohr T, Becker C, Knez A, Kopp A F, Fukuda K and Reiser M F 2000 Cardiac imaging with retrospectively ECG-gated fast multi-slice spiral CT *Radiologe* **40** 111–7

Orecchia R *et al* 2007 Intraoperative radiotherapy for locally advanced prostate cancer: treatment technique and ultra sound-based analysis of dose distribution *Anticancer Res.* **27** 3471–6

Ozhasoglu C and Murphy M J 2002 Issues in respiratory motion compensation during external-beam radiotherapy *Int. J. Radiat. Oncol. Biol. Phys.* **52** 1389–99

Padhani A R, Khoo V S, Suckling J, Husband J E, Leach M O and Dearnaley D P 1999 Evaluating the effect of rectal distension and rectal movement on prostate gland position using cine MRI *Int. J. Radiat. Oncol. Biol. Phys.* **44** 525–33

Pagoulatos N, Haynor D R and Kim Y 2001 A fast calibration method for 3-D tracking of ultrasound images using a spatial localizer *Ultrasound Med. Biol.* **27** 1219–29

Pang G and Rowlands J A 2002 Development of high quantum efficiency flat panel detectors for portal imaging: intrinsic spatial resolution *Med. Phys.* **29** 2274–85

Parent L, Seco J, Evans P M, Fielding A and Dance D R 2006 Monte Carlo modelling of a-Si EPID response: the effect of spectral variations with field size and position *Med. Phys.* **33** 4527–40

Parker R P, Hobday P A and Cassell K J 1979 Direct use of CT numbers in radiotherapy dosage calculations for inhomogeneous-media *Phys. Med. Biol.* **24** 802–9

Pasma K L, Kroonwijk M, Quint S, Visser A G and Heijmen B J M 1999 Transit dosimetry with an electronic portal imaging device (EPID) for 115 prostate cancer patients *Int. J. Radiat. Oncol. Biol. Phys.* **45** 1297–303

Payne G S and Leach M O 2006 Applications of magnetic resonance spectroscopy in radiotherapy treatment planning *Br. J. Radiol.* **79** S16–26

Peignaux K, Truc G, Barillot I, Ammor A, Naudy S, Crehange G and Maingon P 2006 Clinical assessment of the use of the Sonarray system for daily prostate localization *Radiother. Oncol.* **81** 176–8

Petersch B, Bogner J, Fransson A, Lorang T and Potter R 2004 Effects of geometric distortion in 0.2 T MRI on radiotherapy treatment planning of prostate cancer *Radiother. Oncol.* **71** 55–64

Pisani L, Lockman D, Jaffray D, Yan D, Martinez A and Wong J 2000 Setup error in radiotherapy: on-line correction using electronic kilovoltage and megavoltage radiographs *Int. J. Radiat. Oncol. Biol. Phys.* **47** 825–39

Ploeger L S, Frenay M, Betgen A, de Bois J A, Gilhuijs K G A and van Herk M 2003 Application of video imaging for improvement of patient set-up *Radiother. Oncol.* **68** 277–84

Poggi M M, Gant D A, Sewchand W and Warlick W B 2003 Marker seed migration in prostate localization *Int. J. Radiat. Oncol. Biol. Phys.* **56** 1248–51

Pos F J, Hulshof M, Lebesque J, Lotz H, van Tienhoven G R, Moonen L and Remeijer P 2006 Adaptive radiotherapy for invasive bladder cancer: a feasibility study *Int. J. Radiat. Oncol. Biol. Phys.* **64** 862–8

Pouliot J *et al* 2005 Low-dose megavoltage cone-beam CT for radiation therapy *Int. J. Radiat. Oncol. Biol. Phys.* **61** 552–60

Pouliot J, Sonke J, Tome W, Lagendijk J, Brock K, Kessler M and Siewerdsen J 2007 The great debate: the future of IGRT is . . . Megavolt CT . . . Kilovoltage CT . . . Ultrasound-based hybrids . . . MRI guidance . . . 3D deformable image registration *Med. Phys.* **34** 2556–7

Prager R, Gee A, Treece G and Berman L 2002 Freehand 3D ultrasound without voxels: volume measurement and visualisation using the Stradx system *Ultrasonics* **40** 109–15

Prott F J, Haverkamp U, Eich H, Resch A, Micke O, Fischedick A R, Willich N and Potter R 2000 Effect of distortions and asymmetry in MR images on radiotherapeutic treatment planning *Int. J. Cancer* **90** 46–50

Raaymakers B W, Raaijmakers A J E, Kotte A N T J, Jette D and Lagendijk J J W 2004 Integrating a MRI scanner with a 6 MV radiotherapy accelerator: dose deposition in a transverse magnetic field *Phys. Med. Biol.* **49** 4109–18

Rasch C, Barillot I, Remeijer P, Touw A, van Herk M and Lebesque J V 1999 Definition of the prostate in CT and MRI: a multi-observer study *Int. J. Radiat. Oncol. Biol. Phys.* **43** 57–66

Remouchamps V M, Vicini F A, Sharpe M B, Kestin L L, Martinez A A and Wong J W 2003 Significant reductions in heart and lung doses using deep inspiration breath hold with active breathing control and intensity-modulated radiation therapy for patients treated with locoregional breast irradiation *Int. J. Radiat. Oncol. Biol. Phys.* **55** 392–406

Reynaert N, van der Marck S C, Schaart D R, Van der Zee W, Van Vliet-Vroegindeweij C, Tomsej M, Jansen J, Heijmen B, Coghe M and De Wagter C 2007 Monte Carlo treatment planning for photon and electron beams *Radiat. Phys. Chem.* **76** 643–86

Reynaert N, Van Eijkeren M, Taeymans Y and Thierens H 2001 Dosimetry of Ir-192 sources used for endovascular brachytherapy *Phys. Med. Biol.* **46** 499–516

Rietzel E, Chen G T Y, Choi N C and Willet C G 2005a Four-dimensional image-based treatment planning: Target volume segmentation and dose calculation in the presence of respiratory motion *Int. J. Radiat. Oncol. Biol. Phys.* **61** 1535–50

Rietzel E, Liu A K, Doppke K P, Wolfgang J A, Chen A B, Chen G T Y and Choi N C 2006 Design of 4D treatment planning target volumes *Int. J. Radiat. Oncol. Biol. Phys.* **66** 287–95

Rietzel E, Pan T S and Chen G T Y 2005b Four-dimensional computed tomography: image formation and clinical protocol *Med. Phys.* **32** 874–89

Roach M, FaillaceAkazawa P, Malfatti C, Holland J and Hricak H 1996 Prostate volumes defined by magnetic resonance imaging and computerized tomographic scans for three-dimensional conformal radiotherapy *Int. J. Radiat. Oncol. Biol. Phys.* **35** 1011–8

Roach M, Pickett B, Holland J, Zapotowski K A, Marsh D L and Tatera B S 1993 The role of the urethrogram during simulation for localized prostate-cancer *Int. J. Radiat. Oncol. Biol. Phys.* **25** 299–307

Rouviere O, Valette O, Grivolat S, Colin-Pangaud C, Bouvier R, Chapelon Y, Gelet A and Lyonnet D 2004 Recurrent prostate cancer after external beam radiotherapy: value of contrast-enhanced dynamic MRI in localizing intraprostatic tumor correlation with biopsy findings *Urology* **63** 922–7

Ruchala K J, Olivera G H, Schloesser E A and Mackie T R 1999 Megavoltage CT on a tomotherapy system *Phys. Med. Biol.* **44** 2597–621

Rueckert D, Sonoda L I, Hayes C, Hill D L G, Leach M O and Hawkes D J 1999 Nonrigid registration using free-form deformations: application to breast MR images *IEEE Trans. Med. Imaging* **18** 712–21

Sahinler I, Cepni I, Oksuz D C, Cepni K, Koksal S, Koca A, Atkovar G and Okkan S 2004 Tandem application with transvaginal ultrasound guidance *Int. J. Radiat. Oncol. Biol. Phys.* **59** 190–6

Sawada A, Yoda K, Kokubo M, Kunieda T, Nagata Y and Hiraoka M 2004 A technique for noninvasive respiratory gated radiation treatment system based on a real time 3D ultrasound image correlation: A phantom study *Med. Phys.* **31** 245–50

Sawant A, Antonuk L E, El-Mohri Y, Li Y X, Su Z, Wang Y, Yamamoto J, Zhao Q H, Du H, Daniel J and Street R 2005 Segmented phosphors; MEMS-based high quantum efficiency detectors for megavoltage x-ray imaging *Med. Phys.* **32** 553–65

Sawant A, Zeman H, Samant S, Lovhoiden G, Weinberg B and DiBianca F 2002 Theoretical analysis and experimental evaluation of a CsI(Tl) based electronic portal imaging system *Med. Phys.* **29** 1042–53

Schneider U, Pedroni E and Lomax A 1996 The calibration of CT Hounsfield units for radiotherapy treatment planning *Phys. Med. Biol.* **41** 111–24

Schoffel P J, Harms W, Sroka-Perez G, Schlegel W and Karger C P 2007 Accuracy of a commercial optical 3D surface imaging system for realignment of patients for radiotherapy of the thorax *Phys. Med. Biol.* **52** 3949–63

Schreibmann E, Chen G T Y and Xing L 2006 Image interpolation in 4D CT using a BSpline deformable registration model *Int. J. Radiat. Oncol. Biol. Phys.* **64** 1537–50

Seco J and Evans P M 2006 Assessing the effect of electron density in photon dose calculations *Med. Phys.* **33** 540–52

Seco J, Sharp G C, Turcotte J, Gierga D, Bortfeld T and Paganetti H 2007 Effects of organ motion on IMRT treatments with segments of few monitor units *Med. Phys.* **34** 923–34

Seppenwoolde Y, Berbeco R I, Nishioka S, Shirato H and Heijmen B 2007 Accuracy of tumor motion compensation algorithm from a robotic respiratory tracking system: a simulation study *Med. Phys.* **34** 2774–84

Seppenwoolde Y, Shirato H, Kitamura K, Shimizu S, van Herk M, Lebesque J V and Miyasaka K 2002 Precise and real-time measurement of 3D tumor motion in lung due to breathing and heartbeat, measured during radiotherapy *Int. J. Radiat. Oncol. Biol. Phys.* **53** 822–34

Seppi E J *et al* 2003 Megavoltage cone-beam computed tomography using a high-efficiency image receptor *Int. J. Radiat. Oncol. Biol. Phys.* **55** 793–803

Shen S, Duan J, Fiveash J B, Brezovich I A, Plant B A, Spencer S A, Popple R A, Pareek P N and Bonner J A 2003 Validation of target volume and position in respiratory gated CT planning and treatment *Med. Phys.* **30** 3196–205

Sherouse G W, Novins K and Chaney E L 1990 Computation of digitally reconstructed radiographs for use in radiotherapy treatment design *Int. J. Radiat. Oncol. Biol. Phys.* **18** 651–8

Shimizu S, Shirato H, Ogura S, Akita-Dosaka H, Kitamura K, Nishioka T, Kagei K, Nishimura M and Miyasaka K 2001 Detection of lung tumor movement in real-time tumor-tracking radiotherapy *Int. J. Radiat. Oncol. Biol. Phys.* **51** 304–10

Shirato H *et al* 2000a Four-dimensional treatment planning and fluoroscopic real-time tumor tracking radiotherapy for moving tumor *Int. J. Radiat. Oncol. Biol. Phys.* **48** 435–42

Shirato H *et al* 2000b Physical aspects of a real-time tumor-tracking system for gated radiotherapy *Int. J. Radiat. Oncol. Biol. Phys.* **48** 1187–95

Shirato H, Oita M, Fujita K, Watanabe Y and Miyasaka K 2004a Feasibility of synchronization of real-time tumor-tracking radiotherapy and intensity-modulated radiotherapy from viewpoint of excessive dose from fluoroscopy *Int. J. Radiat. Oncol. Biol. Phys.* **60** 335–41

Shirato H, Seppenwoolde Y, Kitamura K, Onimura R and Shimizu S 2004b Intrafractional tumor motion: lung and liver *Semin. Radiat. Oncol.* **14** 10–8

Shirato H *et al* 2006 Speed and amplitude of lung tumor motion precisely detected in four-dimensional setup and in real-time tumor-tracking radiotherapy *Int. J. Radiat. Oncol. Biol. Phys.* **64** 1229–36

Sidhu K *et al* 2003 Optimization of conformal thoracic radiotherapy using cone-beam CT imaging for treatment verification *Int. J. Radiat. Oncol. Biol. Phys.* **55** 757–67

Sidhu K, Cooper P, Ramani R, Schwartz M, Franssen E and Davey P 2004 Delineation of brain metastases on CT images for planning radiosurgery: concerns regarding accuracy *Br. J. Radiol.* **77** 39–42

Siebers J V, Kim J O, Ko L, Keall P J and Mohan R 2004 Monte Carlo computation of dosimetric amorphous silicon electronic portal images *Med. Phys.* **31** 2135–46

Siewerdsen J H and Jaffray D A 2001 Cone-beam computed tomography with a flat-panel imager: magnitude and effects of x-ray scatter *Med. Phys.* **28** 220–31

Siewerdsen J H, Moseley D J, Bakhtiar B, Richard S and Jaffray D A 2004 The influence of antiscatter grids on soft-tissue detectability in cone-beam computed tomography with flat-panel detectors *Med. Phys.* **31** 3506–20

Sillanpaa J, Chang J, Mageras G, Riem H, Ford E, Todor D, Ling C C and Amols H 2005 Developments in megavoltage cone beam CT with an amorphous silicon EPID: reduction of exposure and synchronization with respiratory gating *Med. Phys.* **32** 819–29

Simpson R G, Chen C T, Grubbs E A and Swindell W 1982 A 4-MV CT scanner for radiation-therapy—the prototype system *Med. Phys.* **9** 574–9

Sixel K E, Ruschin M, Tirona R and Cheung P C F 2003 Digital fluoroscopy to quantify lung tumor motion: potential for patient-specific planning target volumes *Int. J. Radiat. Oncol. Biol. Phys.* **57** 717–23

Soete G, Van de Steene J, Verellen D, Vinh-Hung V, Van den Berge D, Michielsen D, Keuppens F, De Roover P and Storme G 2002 Initial clinical experience with infrared-reflecting skin markers in the positioning of patients treated by conformal radiotherapy for prostate cancer *Int. J. Radiat. Oncol. Biol. Phys.* **52** 694–8

Sonke J J, Zijp L, Remeijer P and van Herk M 2005 Respiratory correlated cone beam CT *Med. Phys.* **32** 1176–86

Sontag M R and Cunningham J R 1978 The equivalent tissue-air ratio method for making absorbed dose calculations in a heterogeneous media *Radiology* **129** 787–94

Spezi E and Lewis D G 2002 Full forward Monte Carlo calculation of portal dose from MLC collimated treatment beams *Phys. Med. Biol.* **47** 377–90

Spies L, Evans P M, Partridge M, Hansen V N and Bortfeld T 2000 Direct measurement and analytical modeling of scatter in portal imaging *Med. Phys.* **27** 462–71

Stock R G, Chan K, Terk M, Dewyngaert J K, Stone N N and Dottino P 1997 A new technique for performing Syed-Neblett template interstitial implants for gynecologic malignancies using transrectal-ultrasound guidance *Int. J. Radiat. Oncol. Biol. Phys.* **37** 819–25

Storaas T, Gjesdal K I, Svindland A, Viktil E and Geitung J T 2004 Dynamic first pass 3D EPI of the prostate: accuracy in tumor location *Acta Radiol.* **45** 584–90

Stroom J C, de Boer H C J, Huizenga H and Visser A G 1999 Inclusion of geometrical uncertainties in radiotherapy treatment planning by means of coverage probability *Int. J. Radiat. Oncol. Biol. Phys.* **43** 905–19

Sumi M, Sakihama N, Sumi T, Morikawa M, Uetani M, Kabasawa H, Shigeno K, Hayashi K, Takahashi H and Nakamura T 2003 Discrimination of metastatic cervical lymph nodes with diffusion-weighted MR imaging in patients with head and neck cancer *Am. J. Neuroradiol.* **24** 1627–34

Swindell W 1983 A 4-MV CT scanner for radiation-therapy—spectral properties of the therapy beam *Med. Phys.* **10** 347–51

Sykes J R, Amer A, Czajka J and Moore C J 2005 A feasibility study for image guided radiotherapy using low dose, high speed, cone beam X-ray volumetric imaging *Radiother. Oncol.* **77** 45–52

Tan P N, Steinbach M and Kumar V 2005 *Introduction to Data Mining* (Boston: Addison-Wesley Longman)

Tanner S F, Finnigan D J, Khoo V S, Mayles P, Dearnaley D P and Leach M O 2000 Radiotherapy planning of the pelvis using distortion corrected MR images: the removal of system distortions *Phys. Med. Biol.* **45** 2117–32

Teefey S A *et al* 2003 Detection of primary hepatic malignancy in liver transplant candidates: prospective comparison of CT, MR imaging US and PET *Radiology* **226** 533–42

Ten Haken R K, Thornton A F, Sandler H M, Lavigne M L, Quint D J, Fraass B A, Kessler M L and McShan D L 1992 A quantitative assessment of the addition of mri to ct-based, 3-d treatment planning of brain-tumors *Radiother. Oncol.* **25** 121–33

Treece G M, Gee A H, Prager R W, Cash C J C and Berman L H 2003 High-definition freehand 3-D ultrasound *Ultrasound Med. Biol.* **29** 529–46

Treece G M, Prager R W, Gee A H and Berman L 2002 Correction of probe pressure artifacts in freehand 3D ultrasound *Med. Image Anal.* **6** 199–214

Trichter F and Ennis R D 2003 Prostate localization using transabdominal ultrasound imaging *Int. J. Radiat. Oncol. Biol. Phys.* **56** 1225–33

Underberg R W M, Lagerwaard F J, Cuijpers J P, Slotman B J, de Koste J R V and Senan S 2004 Four-dimensional ct scans for treatment planning in stereotactic radiotherapy for stage I lung cancer *Int. J. Radiat. Oncol. Biol. Phys.* **60** 1283–90

Van de Steene J, Linthout N, de Mey J, Vinh-Hung V, Claassens C, Noppen M, Bel A and Storme G 2002 Definition of gross tumor volume in lung cancer: inter-observer variability *Radiother. Oncol.* **62** 37–49

Van den Heuvel F, Powell T, Seppi E, Littrupp P, Khan M, Wang Y and Forman J D 2003 Independent verification of ultrasound based image-guided radiation treatment, using electronic portal imaging and implanted gold markers *Med. Phys.* **30** 2878–87

van der Geld Y G, Senan S, de Koste J R V, van Tinteren H, Slotman B J, Underberg R W M and Lagerwaard F J 2006 Evaluating mobility for radiotherapy planning of lung tumors: a comparison of virtual fluoroscopy and 4D CT *Lung Cancer* **53** 31–7

Van Esch A, Depuydt T and Huyskens D P 2004 The use of an aSi-based EPID for routine absolute dosimetric pre-treatment verification of dynamic IMRT fields *Radiother. Oncol.* **71** 223–34

van Herk M 2004 Errors and margins in radiotherapy *Semin. Radiat. Oncol.* **14** 52–64

Van Herk M and Lomax A 2007 Have we forgotten about the ALARA principle in IGRT? *Radiother. Oncol.* **84** S54

van Herk M, Remeijer P, Rasch C and Lebesque J V 2000 The probability of correct target dosage: dose-population histograms for deriving treatment margins in radiotherapy *Int. J. Radiat. Oncol. Biol. Phys.* **47** 1121–35

Vedam S S, Keall P J, Kini V R and Mohan R 2001 Determining parameters for respiration-gated radiotherapy *Med. Phys.* **28** 2139–46

Verhaegen F and Devic S 2005 Sensitivity study for CT image use in Monte Carlo treatment planning *Phys. Med. Biol.* **50** 937–46

Verhaegen F and Seuntjens J 2003 Monte Carlo modelling of external radiotherapy photon beams *Phys. Med. Biol.* **48** R107–64

Vigneault E, Pouliot J, Laverdiere J, Roy J and Dorion M 1997 Electronic portal imaging device detection of radioopaque markers for the evaluation of prostate position during megavoltage irradiation: a clinical study *Int. J. Radiat. Oncol. Biol. Phys.* **37** 205–12

Wagman R, Yorke E, Ford E, Giraud P, Mageras G, Minsky B and Rosenzweig K 2003 Respiratory gating for liver tumors: use in dose escalation *Int. J. Radiat. Oncol. Biol. Phys.* **55** 659–68

Wang D, Strugnell W, Cowin G, Doddrell D M and Slaughter R 2004a Geometric distortion in clinical MRI systems—Part I: evaluation using a 3D phantom *Magn. Reson. Imaging* **22** 1211–21

Wang D, Strugnell W, Cowin G, Doddrell D M and Slaughter R 2004b Geometric distortion in clinical MRI systems—Part II: correction using a 3D phantom *Magn. Reson. Imaging* **22** 1223–32

Wang D M, Doddrell D M and Cowin G 2004c A novel phantom and method for comprehensive 3-dimensional measurement and correction of geometric distortion in magnetic resonance imaging *Magn. Reson. Imaging* **22** 529–42

Wang Y, Cardinal N, Downey D B and Fenster A 2003 Semiautomatic three-dimensional segmentation of the prostate using two-dimensional ultrasound images *Med. Phys.* **30** 887–97

Warkentin B, Steciw S, Rathee S and Fallone B G 2003 Dosimetric IMRT verification with a flat-panel EPID *Med. Phys.* **30** 3143–55

Webb S 1989 Optimization of conformal radiotherapy dose distributions by simulated annealing *Phys. Med. Biol.* **34** 1349–70

Webb S 1993 *The Physics of Three-dimensional Radiation Therapy* (London: Taylor and Francis) chapter 1

Webb S 2000 *Intensity Modulated Radiation Therapy* (London: Taylor and Francis)

Webb S 2005 The effect on IMRT conformality of elastic tissue movement and a practical suggestion for movement compensation via the modified dynamic multileaf collimator (dMLC) technique *Phys. Med. Biol.* **50** 1163–90

Webb S 2008 Adapting IMRT delivery fraction-by-fraction to cater for variable intrafraction motion *Phys. Med. Biol.* **53** 1–21

Weiss E, Richter S, Krauss T, Metzelthin S I, Hille A, Pradier O, Siekmeyer B, Vorwerk H and Hess C F 2003 Conformal radiotherapy planning of cervix carcinoma: differences in the delineation of the clinical target volume. A comparison between gynaecologic and radiation oncologists *Radiother. Oncol.* **67** 87–95

Weltens C, Menten J, Feron M, Bellon E, Demaerel P, Maes F, Van den Bogaert W and van der Schueren E 2001 Interobserver variations in gross tumor volume delineation of brain tumors on computed tomography and impact of magnetic resonance imaging *Radiother. Oncol.* **60** 49–59

Wendling M, Louwe R J W, McDermott L N, Sonke J J, van Herk M and Mijnheer B J 2006 Accurate two-dimensional IMRT verification using a back-projection EPID dosimetry method *Med. Phys.* **33** 259–73

Wenz F, Rempp K, Hess T, Debus J, Brix G, Engenhart R, Knopp M V, van Kaick G and Wannenmacher M 1996 Effect of radiation on blood volume in low-grade astrocytomas and normal brain tissue: quantification with dynamic susceptibility contrast MR imaging *Am. J. Roentgenol.* **166** 187–93

White E A, Cho J, Vallis K A, Sharpe M B, Lee G, Blackburn H, Nageeti T, McGibney C and Jaffray D A 2007 Cone beam computed tomography guidance for setup of patients receiving accelerated partial breast irradiation *Int. J. Radiat. Oncol. Biol. Phys.* **68** 547–54

Wilks R J and Bliss P 2002 The use of a compensator library to reduce dose inhomogeneity in tangential radiotherapy of the breast *Radiother. Oncol.* **62** 147–57

Willoughby T R *et al* 2006 Target localization and real-time tracking using the calypso 4D localization system in patients with localized prostate cancer *Int. J. Radiat. Oncol. Biol. Phys.* **65** 528–34

Winkler P, Hefner A and Georg D 2005 Dose-response characteristics of an amorphous silicon EPID *Med. Phys.* **32** 3095–105

Wolthaus J W H *et al* 2006 Mid-ventilation CT scan construction from four-dimensional respiration-correlated CT scans for radiotherapy planning of lung cancer patients *Int. J. Radiat. Oncol. Biol. Phys.* **65** 1560–71

Wolthaus J W H, van Herk M, Muller S H, Belderbos J S A, Lebesque J V, de Bois J A, Rossi M M G and Damen E M F 2005 Fusion of respiration-correlated PET and CT scans: correlated lung tumour motion in anatomical and functional scans *Phys. Med. Biol.* **50** 1569–83

Wong J W, Sharpe M B, Jaffray D A, Kini V R, Robertson J M, Stromberg J S and Martinez A A 1999 The use of active breathing control (ABC) to reduce margin for breathing motion *Int. J. Radiat. Oncol. Biol. Phys.* **44** 911–9

Wurstbauer K, Deutschmann H, Kopp P and Sedlmayer F 2005 Radiotherapy planning for lung cancer: Slow CTs allow the drawing of tighter margins *Radiother. Oncol.* **75** 165–70

Yan D, Ziaja E, Jaffray D, Wong J, Brabbins D, Vicini F and Martinez A 1998 The use of adaptive radiation therapy to reduce setup error: a prospective clinical study *Int. J. Radiat. Oncol. Biol. Phys.* **41** 715–20

Yan Y L, Song Y L and Boyer A L 2002 An investigation of a video-based patient repositioning technique *Int. J. Radiat. Oncol. Biol. Phys.* **54** 606–14

Yarnold J, Ashton A, Bliss J, Homewood J, Harper C, Hanson J, Haviland J, Bentzen S and Owen R 2005 Fractionation sensitivity and dose response of late adverse effects in the breast after radiotherapy for early breast cancer: long-term results of a randomised trial *Radiother. Oncol.* **75** 9–17

Yin F F *et al* 2002 A technique of intensity-modulated radiosurgery (IMRS) for spinal tumors *Med. Phys.* **29** 2815–22

Yin F F, Guan H Q and Lu W K 2005 A technique for on-board CT reconstruction using both kilovoltage and megavoltage beam projections for 3D treatment verification *Med. Phys.* **32** 2819–26

Yoo S, Kim G Y, Hammoud R, Elder E, Pawlicki T, Guan H Q, Fox T, Luxton G, Yin F F and Munro P 2006 A quality assurance program for the on-board imager *Med. Phys.* **33** 4431–47

Yoo S and Yin F F 2006 Dosimetric feasibility of cone-beam CT-based treatment planning compared to CT-based treatment planning *Int. J. Radiat. Oncol. Biol. Phys.* **66** 1553–61

Zamorano L, Dujovny M, Malik G, Yakar D and Mehta B 1987 Multiplanar CT-guided stereotaxis and I125 interstitial radiotherapy—image-guided tumor volume assessment, planning, dosimetric calculations, stereotactic biopsy and implantation of removable catheters *Appl. Neurophysiol.* **50** 281–6

Zhang Y B, Zhang L F, Zhu R, Lee A K, Chambers M and Dong L 2007 Reducing metal artifacts in cone-beam CT images by preprocessing projection data *Int. J. Radiat. Oncol. Biol. Phys.* **67** 924–32

Zhao H, Hubenschmidt J, Malinowski K and Parikh P 2007 Initial phantom evaluation of a surface imaging system (GateCT®) for 4-D CT *Med. Phys.* **34** 2554